Instanton and noninstanton tunneling in periodically perturbed barriers: Semiclassical and quantum interpretations

Kin'ya Takahashi
The Physics Laboratories, Kyushu Institute of Technology, Kawazu 680-4, Iizuka 820-8502, Japan

Kensuke S. Ikeda
Department of Physics, Ritsumeikan University, Noji-higashi 1-1-1, Kusatsu 525-8577, Japan
(Received 12 August 2012; published 13 November 2012)

In multidimensional barrier tunneling, there exist two different types of tunneling mechanisms, instanton-type tunneling and noninstanton tunneling. In this paper we investigate transitions between the two tunneling mechanisms from the semiclassical and quantum viewpoints taking two simple models: a periodically perturbed Eckart barrier for the semiclassical analysis and a periodically perturbed rectangular barrier for the quantum analysis. As a result, similar transitions are observed with change of the perturbation frequency ω for both systems, and we obtain a comprehensive scenario from both semiclassical and quantum viewpoints for them. In the middle range of ω, in which the plateau spectrum is observed, noninstanton tunneling dominates the tunneling process, and the tunneling amplitude takes the maximum value. Noninstanton tunneling explained by stable-unstable manifold guided tunneling (SUMGT) from the semiclassical viewpoint is interpreted as multiphoton-assisted tunneling from the quantum viewpoint. However, in the limit $\omega \to 0$, instanton-type tunneling takes the place of noninstanton tunneling, and the tunneling amplitude converges on a constant value depending on the perturbation strength. The spectrum localized around the input energy is observed, and there is a scaling law with respect to the width of the spectrum envelope, i.e., the width $\propto \hbar\omega$. In the limit $\omega \to \infty$, the tunneling amplitude converges on that of the unperturbed system, i.e., the instanton of the unperturbed system.

DOI: 10.1103/PhysRevE.86.056206 PACS number(s): 05.45.Mt, 03.65.Xp, 03.65.Sq

I. INTRODUCTION

During the last few decades, understanding quantum tunneling in multidimensional systems has been a crucial problem in the field of quantum chaos as well as many other fields, e.g., quantum chemistry, nanoscale semiconductor devices, and so on. From the viewpoint of quantum chaos, various novel tunneling phenomena, mostly categorized into dynamical tunneling, have been predicted, found, and observed theoretically, numerically and experimentally, e.g., chaos-assisted tunneling, resonance-assisted tunneling, and Julia set-assisted tunneling [1–15]. The basic mechanisms of those tunneling phenomena [1–7,9–19] are essentially different from that of instanton-type tunneling, which is the basic tunneling mechanism in one-dimensional systems as well as classically integrable and nearly integrable multidimensional systems [20]. Those noninstanton tunneling phenomena have been interpreted in various ways from semiclassical and quantum points of view and further from hybrid viewpoints [1–7,9–19]. It will be expected that analytical methods developed in different ways become to complement each other and allow us to comprehend all the aspects of multidimensional tunneling.

For multidimensional barrier systems, there exists a tunneling phenomenon different from instanton-type tunneling (barrier penetration) [7,13–16]. In recent works [13–16], we have provided its semiclassical interpretation. It was later reconfirmed in a slightly different way [21]. In this semiclassical mechanism, stable and unstable manifolds in the complex domain play an important role in the tunneling process, namely, complex trajectories contributing to tunneling are guided by complex stable and unstable manifolds of an unstable periodic orbit above the top of a potential barrier. For brevity, it is called stable-unstable manifold guided tunneling (SUMGT). SUMGT is essentially the same as Julia set-assisted tunneling introduced by Shudo *et al.* in which forward and backward Julia sets, almost equivalent to complex stable and unstable manifolds [12], guide tunneling trajectories even in the case that chaos exists in the real space [11,12], although they studied tunneling in discrete time systems.

In relatively low-frequency ranges for periodically perturbed barrier systems, two types of tunneling mechanisms, instanton-type tunneling and SUMGT, simultaneously contribute to the tunneling process, and the winner of the competition between them dominates the tunneling process [16,17]. In the limit that the frequency ω goes to zero, the tunneling amplitude converges on a constant value depending on the strength of perturbation ϵ, which can be estimated by an adiabatic perturbation method based on the instanton theory. As a result, a localized tunneling spectrum around the input energy is observed. However, the contribution of SUMGT rapidly grows with increase of ω and overwhelms instanton-type tunneling. SUMGT causes a different type of the tunneling spectrum, the so-called plateau spectrum, which spreads over a wide range of energy with its center at the height of the potential barrier at rest. The tunneling amplitude ruled by SUMGT takes the maximum value in a middle frequency range. In the relatively high-frequency range, in which the semiclassical method cannot be applied, the tunneling amplitude decreases with increase of ω and finally converges on that of the unperturbed barrier, which is estimated by

the instanton. Essentially the same change of the tunneling amplitude with the perturbation frequency was reported in the case that the wave packet collides with a oscillating potential barrier [22], though it gave an intuitive explanation.

By using periodically perturbed step potentials, we can investigate characteristics of pure noninstanton tunneling, because instanton-type tunneling is substantially prohibited [18,19]. A periodically perturbed rounded of-step potential is suitable for the semiclassical analysis [18,19], while a periodically perturbed right-angled step potential is appropriate for the analysis from the quantum viewpoint [19], because the solution is written in an exact form, which can be numerically solved without any perturbation. Noninstanton tunneling observed for both systems takes the maximum tunneling amplitude in the middle-frequency range but decays toward zero in both low- and high-frequency limits, $\omega \to 0$ and $\omega \to \infty$. In a relatively low-frequency range, noninstanton tunneling caused by SUMGT is explained by the multiphoton-assisted tunneling from the quantum viewpoint. In the high-frequency range in which the semiclassical method, i.e., SUMGT, cannot be applied due to large values of $\hbar\omega$, a single quantum (or a few quanta) absorption mainly contributes to the tunneling process.

In this paper we developed our study in this direction to the case of the periodically perturbed barriers. We investigate tunneling through a periodically perturbed rectangular barrier for the purely quantum analysis compared with the semiclassical analysis of tunneling through a periodically perturbed rounded-off potential barrier. As with the periodically perturbed right-angled step potential, so the periodically perturbed rectangular barrier has a solution written by an exact form, which can be numerically solved without any perturbation [23,24]. It is very helpful for us to give the quantum interpretations of noninstanton tunneling and instanton-type tunneling. Many authors have studied tunneling phenomena of periodically perturbed barriers [22–27]. However, to the best knowledge of the authors of this paper, there have been few works which explore noninstanton tunneling compared with instanton-type tunneling in order to obtain comprehensive understanding from both quantum and semiclassical viewpoints, especially in the low and middle-frequency regimes. We clarify the difference between the two types of tunneling mechanisms and investigate transitions between them with change of the perturbation frequency from both quantum and semiclassical viewpoints. It is expected that those approaches provide a more complete understanding of tunneling mechanisms in multidimensional systems.

This paper is organized as follows. In Sec. II we introduce the periodically perturbed Eckart potential as a smooth potential model and show the outline of the change of tunneling mechanism between instanton-type tunneling and noninstanton tunneling with change of the perturbation frequency. In Sec. III we introduce the periodically perturbed rectangular barrier and give quantum explanations for both tunneling mechanisms, which clarify how the change of tunneling mechanism occurs with change of the perturbation frequency. In Sec. IV we show alternative explanations for both tunneling mechanisms from the semiclassical viewpoint compered with the pure quantum explanations. Section V is devoted to discussion.

II. TUNNELING IN PERIODICALLY PERTURBED ROUNDED OFF BARRIER

In this section we show the outline of tunneling observed for the periodically perturbed rounded-off barrier reported in our recent works [13–17]. The model system is the periodically perturbed Eckart barrier:

$$H(Q,P,\omega t) = \tfrac{1}{2}P^2 + (1+\epsilon\sin\omega t)\mathrm{sech}^2 Q. \qquad (1)$$

Let us assume that a plane wave is incident on this potential with input energy $E_I(<1-\epsilon)$ at which only a tunneling wave is observed in the transmissive side. For quantum calculations, we have used the numerical scheme developed by ourselves [28] based on Miller's (quantum) S-matrix formula [29], which generates an incident plane wave at a high degree of accuracy with exponentially small errors so that a scattering eigenstate is obtained numerically.

The feature of the tunneling spectrum changes with the angular frequency ω as well as the strength ϵ. Figure 1 shows spectra at three representative values of ω.

For a low frequency typically at $\omega = 0.03$ [Fig. 1(a)], spectra are well localized in very small ranges around E_I for all three values of ϵ, i.e., $\epsilon = 0.1, 0.2, 0.4$. These spectra are estimated by an adiabatic approximation based on the instanton as shown later [16,17].

For a middle frequency typically at $\omega = 0.3$ [Fig. 1(b)], the spectrum at $\epsilon = 0.4$ is markedly different in shape from the spectra in the low-frequency range, and its envelope forms a plateau spreading over a wide range of energy, which nearly corresponds to the oscillating range of the potential height, $1-\epsilon < E < 1+\epsilon$. As reported in the previous works [14–17], this spectrum is the result of SUMGT. On the other hand, the spectrum at $\epsilon = 0.1$ still forms a localized spectrum, but its width becomes wider compared with that at $\omega = 0.03$. The spectrum at $\epsilon = 0.2$ is considered as a superposition of the two characteristic spectra, a head lobe explained by the perturbed instanton theory and a side shoulder formed over an upper range of energy as the result of SUMGT [14–16]. The side shoulder grows with increase of ω, then it changes into a plateau spectrum at higher frequencies. The larger ϵ is, the faster it grows. Hence the spectrum of the strong perturbation first changes from a localized one to a plateau through intermediate spectra accompanied by a side shoulder, and the spectra of the middle and weak perturbations follow successively.

For a high frequency typically at $\omega = 10.0$ [Fig. 1(c)], the peak interval $\hbar\omega$ is larger than the energy difference between the potential height at rest and the input energy, i.e., $1-E_I$, then the semiclassical approximation should not be applicable to this case. The peak heights at the same energy value are not much different for the three values of ϵ. The peak at the first excited energy, i.e., $E = E_I + \hbar\omega$, is larger than others and substantially determines the tunneling amplitude. However, the peaks at excited energy levels rapidly decay with ω, while the fundamental peak at $E = E_I$ converges on that of the unperturbed system. Therefore, the tunneling probability approaches that of the unperturbed system in the limit $\omega \to \infty$ [17,22].

The change of tunneling amplitude, more precisely the maximum value of the peaks of the tunneling spectrum, is

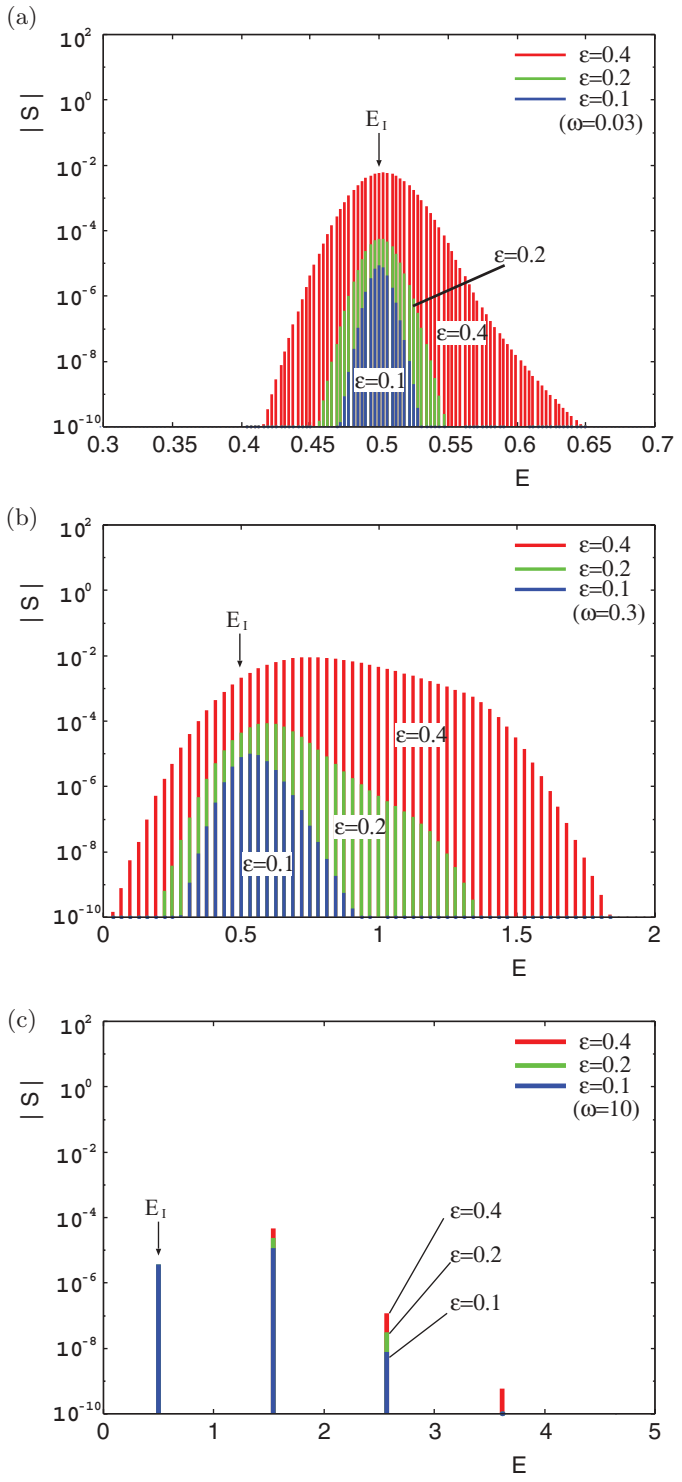

FIG. 1. (Color online) Tunneling spectra of the periodically perturbed Eckart barrier. The input energy is taken at $E_I = 0.5$ and the Planck constant is $\hbar = 1000/(3\pi \times 2^{10}) \sim 0.1036$. The spectrum is normalized such that $\sum_n |S(E = E_I + n\hbar\omega, E_I)|^2$ gives the total transmissive probability. (a) $\omega = 0.03$. (b) $\omega = 0.3$. (c) $\omega = 10$.

summarized in Fig. 2. In the limit $\omega \to 0$, they converge on different values depending on ϵ. The tunneling amplitude grows with increase of ω and takes the maximum value at a certain value of ω depending on ϵ in the middle range. In the

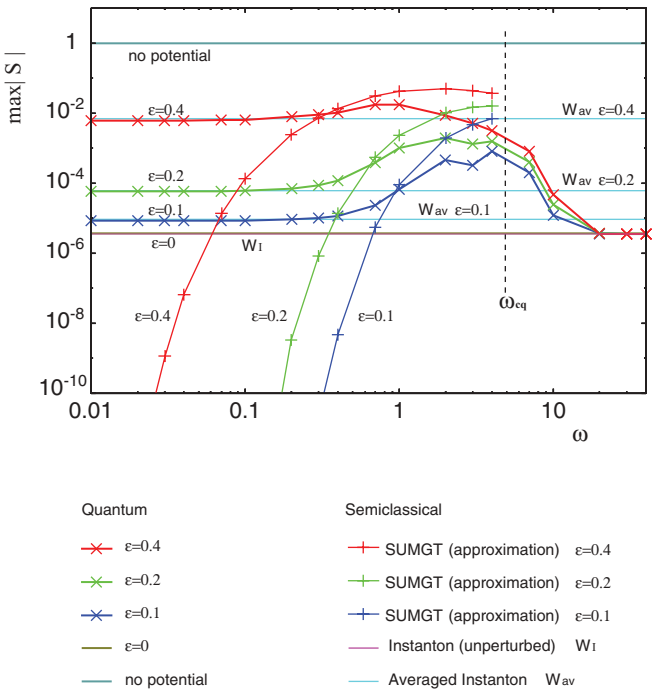

FIG. 2. (Color online) Change of tunneling amplitude (the maximum value of the peaks of the tunneling spectrum) with ω for the periodically perturbed Eckart barrier. The line labeled "SUMGT" is the result of Eq. (67) with Eq. (69), and those labeled "Instanton" and "Averaged instanton" are given by Eq. (57) with Eq. (58) and Eq. (60) with Eq. (59), respectively.

limit $\omega \to \infty$ the tunneling amplitude decays and converges on that of the unperturbed system independently of ϵ, because the perturbation of an extremely high frequency does not substantially affect the system.

Note that essentially the same spectra are observed for a two-dimensional (2D) barrier system [15,30]:

$$H_{\rm tot}(Q,P,q,p) = \tfrac{1}{2}P^2 + (1+\beta q)\,\mathrm{sech}^2 Q + H_{\rm ch}(q,p), \qquad (2)$$

when the channel Hamiltonian,

$$H_{\rm ch} = \tfrac{1}{2}p^2 + \tfrac{1}{2}\omega^2 q^2, \qquad (3)$$

is highly excited. Actually, introducing the action-angle coordinates (I,θ) as canonical coordinates of the channel gives $\beta q = \beta\sqrt{2I/\omega}\cos\theta$, and $\beta\sqrt{2I/\omega}$ plays the same role of ϵ of Eq. (1). If the action I takes large values, the 2D Hamiltonian (2) can be reduced into the periodically perturbed one-dimensional Hamiltonian (1). Therefore, there coexist two tunneling mechanisms, instanton-type tunneling and noninstanton tunneling [especially SUMGT for $\omega < \omega_{\rm cq}(\equiv \frac{1-E_I}{\hbar})$], for the multidimensional potential barriers, and which mechanism dominates the tunneling process changes with initial conditions and control parameters.

III. TUNNELING IN PERIODICALLY PERTURBED RECTANGULAR BARRIER

A. Model system and quantum solution

In this section we give quantum interpretations of instanton-type tunneling and noninstanton tunneling, especially in low

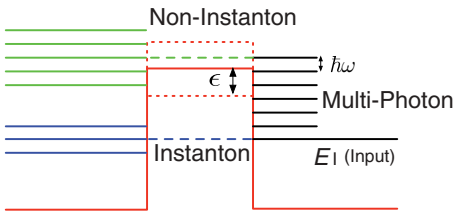

FIG. 3. (Color online) Periodically perturbed rectangular barrier.

and middle frequency ranges. To do this we need a model, which is appropriate for the quantum analysis and exhibits tunneling behavior similar to that of the periodically perturbed rounded-off potential barrier. The model system satisfying our requirement is a periodically perturbed rectangular barrier (see Fig. 3), which has been studied by several authors [23–26]. The Hamiltonian of the model system is

$$H(Q,P,\omega t) = \tfrac{1}{2}P^2 + (1+\epsilon\sin\omega t)[\theta(Q-b_w) - \theta(Q)], \tag{4}$$

where $\theta(x)$ denotes the unit step function, b_w takes a negative value, and $|b_w|$ gives the width of the potential.

Let us consider the situation that a plane wave with input energy E_I is incident on the potential from positive infinity in Q. Then the input, reflective, and transmissive waves are, respectively, written by

$$\Psi_I = \mathrm{e}^{-\frac{i}{\hbar}E_I t}\mathrm{e}^{-\frac{i}{\hbar}P_I Q}, \tag{5}$$

$$\Psi_R = \sum_n \Psi_{rn} = \sum_n R_n \mathrm{e}^{-\frac{i}{\hbar}E_n t}\mathrm{e}^{\frac{i}{\hbar}P_{rn} Q}, \tag{6}$$

$$\Psi_T = \sum_n \Psi_{tn} = \sum_n T_n \mathrm{e}^{-\frac{i}{\hbar}E_n t}\mathrm{e}^{-\frac{i}{\hbar}P_{tn} Q}, \tag{7}$$

where the momentum of the input wave is $P = -P_I = -\sqrt{2E_I} < 0$ and an excited energy level is given by $E_n = E_I + n\hbar\omega$ with the momentum $P = P_{rn} = \sqrt{2E_n} > 0$ for a reflective component and $P = -P_{tn} = -\sqrt{2E_n} < 0$ for a transmissive component.

In the interaction region($b_w < Q < 0$), the left- and right-going waves are, respectively, given by

$$\Psi_{bl} = \sum_n \Psi_{bln} = \sum_n B_{ln}\mathrm{e}^{\frac{i}{\hbar}\frac{\epsilon}{\omega}\cos\omega t}\mathrm{e}^{-\frac{i}{\hbar}E_n t}\mathrm{e}^{-\frac{i}{\hbar}P_{bn} Q}, \tag{8}$$

$$\Psi_{br} = \sum_n \Psi_{brn} = \sum_n B_{rn}\mathrm{e}^{\frac{i}{\hbar}\frac{\epsilon}{\omega}\cos\omega t}\mathrm{e}^{-\frac{i}{\hbar}E_n t}\mathrm{e}^{\frac{i}{\hbar}P_{bn} Q}, \tag{9}$$

where $P_{bn} = \sqrt{2(E_n - 1)}$. The total wave in the interaction region is written by $\Psi_b = \Psi_{bl} + \Psi_{br}$, which is a superposition of the unperturbed solutions modulated by $\mathrm{e}^{\frac{i}{\hbar}\frac{\epsilon}{\omega}\cos\omega t}$ due to the periodical perturbation [23,24]. For $n \geqslant n^*(\equiv \min\{n|E_n > 1\})$, Ψ_{bln} and Ψ_{brn} are plane waves modulated by $\mathrm{e}^{\frac{i}{\hbar}\frac{\epsilon}{\omega}\cos\omega t}$. In the case of $E_n < 1$, namely, $n < n^*$, P_{bn} takes an imaginary value $i\sqrt{2(1-E_n)}$, then Ψ_{bln} and Ψ_{brn} are rewritten by

$$\Psi_{bln} = B_{ln}\mathrm{e}^{\frac{i}{\hbar}\frac{\epsilon}{\omega}\cos\omega t}\mathrm{e}^{-\frac{i}{\hbar}E_n t}\mathrm{e}^{\frac{1}{\hbar}|P_{bn}|Q}, \tag{10}$$

$$\Psi_{brn} = B_{rn}\mathrm{e}^{\frac{i}{\hbar}\frac{\epsilon}{\omega}\cos\omega t}\mathrm{e}^{-\frac{i}{\hbar}E_n t}\mathrm{e}^{-\frac{1}{\hbar}|P_{bn}|Q}, \tag{11}$$

which give barrier-penetrating waves modulated by $\mathrm{e}^{\frac{i}{\hbar}\frac{\epsilon}{\omega}\cos\omega t}$.

The coefficients R_n, T_n, B_{ln}, and B_{rn} are determined with the continuity at the boundaries, $Q = 0$ and $Q = b_w$. The continuity of the wave function at $Q = 0$, i.e., $\Psi_I + \Psi_R = \Psi_{bl} + \Psi_{br}$, is written as

$$1 + \sum_n R_n \mathrm{e}^{-in\omega t} = \sum_n B_{ln}\mathrm{e}^{\frac{i}{\hbar}\frac{\epsilon}{\omega}\cos\omega t}e^{-in\omega t} + \sum_n B_{rn}\mathrm{e}^{\frac{i}{\hbar}\frac{\epsilon}{\omega}\cos\omega t}\mathrm{e}^{-in\omega t}, \tag{12}$$

and the continuous differentiability at $Q = 0$, i.e., $\frac{\partial}{\partial Q}\Psi_I + \frac{\partial}{\partial Q}\Psi_R = \frac{\partial}{\partial Q}\Psi_{bl} + \frac{\partial}{\partial Q}\Psi_{br}$, gives

$$-P_I + \sum_n R_n P_{rn}\mathrm{e}^{-in\omega t} = -\sum_n B_{ln}P_{bn}\mathrm{e}^{\frac{i}{\hbar}\frac{\epsilon}{\omega}\cos\omega t}e^{-in\omega t} + \sum_n B_{rn}P_{bn}\mathrm{e}^{\frac{i}{\hbar}\frac{\epsilon}{\omega}\cos\omega t}\mathrm{e}^{-in\omega t}. \tag{13}$$

In the same way, the continuity of the wave at $Q = b_w = -|b_w|$, i.e., $\Psi_{bl} + \Psi_{br} = \Psi_T$, is expressed as

$$\sum_n T_n \mathrm{e}^{\frac{i}{\hbar}P_{tn}|b_w|}\mathrm{e}^{-in\omega t} = \sum_n B_{ln}\mathrm{e}^{\frac{i}{\hbar}\frac{\epsilon}{\omega}\cos\omega t}\mathrm{e}^{\frac{i}{\hbar}P_{bn}|b_w|}\mathrm{e}^{-in\omega t} + \sum_n B_{rn}\mathrm{e}^{\frac{i}{\hbar}\frac{\epsilon}{\omega}\cos\omega t}\mathrm{e}^{-\frac{i}{\hbar}P_{bn}|b_w|}\mathrm{e}^{-in\omega t}, \tag{14}$$

and the continuous differentiability at $Q = b_w = -|b_w|$, i.e., $\frac{\partial}{\partial Q}\Psi_{bl} + \frac{\partial}{\partial Q}\Psi_{br} = \frac{\partial}{\partial Q}\Psi_T$, provides

$$-\sum_n T_n P_{tn}\mathrm{e}^{\frac{i}{\hbar}P_{tn}|b_w|}\mathrm{e}^{-in\omega t} = -\sum_n B_{ln}P_{bn}\mathrm{e}^{\frac{i}{\hbar}\frac{\epsilon}{\omega}\cos\omega t}\mathrm{e}^{\frac{i}{\hbar}P_{bn}|b_w|}\mathrm{e}^{-in\omega t} + \sum_n B_{rn}P_{bn}\mathrm{e}^{\frac{i}{\hbar}\frac{\epsilon}{\omega}\cos\omega t}\mathrm{e}^{-\frac{i}{\hbar}P_{bn}|b_w|}\mathrm{e}^{-in\omega t}. \tag{15}$$

By using equality [31]

$$\mathrm{e}^{\frac{i}{\hbar}\frac{\epsilon}{\omega}\cos\theta} = \sum_n i^n J_n\left(\frac{\epsilon}{\hbar\omega}\right)\mathrm{e}^{in\theta}, \tag{16}$$

we, after some calculations, obtain the equations for B_{ln} and B_{rn}

$$\sum_m i^{m-n}J_{m-n}\left(\frac{\epsilon}{\hbar\omega}\right)[(P_{rn}+P_{bm})B_{lm} + (P_{rn}-P_{bm})B_{rm}] = 2P_I\delta_{n,0}, \tag{17}$$

$$\sum_m i^{m-n}J_{m-n}\left(\frac{\epsilon}{\hbar\omega}\right)\left[(P_{tn}-P_{bm})\mathrm{e}^{\frac{i}{\hbar}P_{bm}|b_w|}B_{lm} + (P_{tn}+P_{bm})\mathrm{e}^{-\frac{i}{\hbar}P_{bm}|b_w|}B_{rm}\right] = 0. \tag{18}$$

These equations give a closed system of linear equations in B_{ln} and B_{rn}, and then we can obtain B_{ln} and B_{rn} numerically without any perturbation methods. From given B_{ln} and B_{rn},

the coefficients R_n and T_n are straightforwardly obtained as

$$R_n = -\delta_{n,0} + \sum_m (B_{lm} + B_{rm}) i^{m-n} J_{m-n}\left(\frac{\epsilon}{\hbar\omega}\right), \quad (19)$$

$$T_n = e^{-\frac{i}{\hbar}P_{tn}|b_w|}\left[\sum_m i^{m-n} J_{m-n}\left(\frac{\epsilon}{\hbar\omega}\right) \times \left(e^{\frac{i}{\hbar}P_{bm}|b_w|} B_{lm} + e^{-\frac{i}{\hbar}P_{bm}|b_w|} B_{rm}\right)\right]. \quad (20)$$

One can see essentially the same result in Ref. [24].

B. Numerical results

By definition, the transmissive coefficients T_n form the tunneling energy spectrum if the input energy E_I is taken as $E_I < 1 - \epsilon$. As shown in Fig. 4, the tunneling spectra $|T_n|$ are very similar to those of the periodically perturbed Eckart barrier at the same representative values of ω.

At the low frequency $\omega = 0.03$ [Fig. 4(a)], the spectra are well localized in very small ranges around E_I for all the three representative values of ϵ, $\epsilon = 0.1$, 0.2, 0.4. These spectra are very similar to those of the periodically perturbed Eckart barrier at the same value of ω and are well evaluated by an adiabatic approximation as shown later.

At the middle frequency $\omega = 0.3$ [Fig. 4(b)], there exist three different spectra depending on ϵ like those of the periodically perturbed Eckart barrier at the same frequency. At $\epsilon = 0.4$, the spectrum forms a plateau spreading over the range $(1 - \epsilon < E < 1 + \epsilon)$. At $\epsilon = 0.2$, the spectrum is regarded as a mixture of the two characteristic spectra. It has a clearly localized head lobe accompanied by a side shoulder, whose flat part is wider than that of the periodically perturbed Eckart barrier. It means that the separation of the two mechanisms, instanton-type tunneling and noninstanton tunneling, becomes clear for the rectangular barrier compared with the rounded-off barrier. At $\epsilon = 0.1$, a localized spectrum is observed as in the case of the Eckart barrier.

At the high frequency $\omega = 10.0$ [Fig. 4(c)], spectra similar to those of the periodically perturbed Eckart barrier are observed. The peak at the first excited energy, $E = E_I + \hbar\omega$, is larger than the others for all the values of ϵ. The tunneling amplitude is more enhanced by the perturbation; namely, all the peaks are markedly larger than those of the periodically perturbed Eckart barrier.

Figure 5 shows the changes of the tunneling amplitude, namely, the maximum value of $|T_n|$, for (a) $E_I = 0.5$ and (b) $E_I = 0.75$ in the range of ω for which solutions with accuracy are obtained numerically. As in the case of the periodically perturbed Eckart barrier, the tunneling amplitude takes the maximum value in the middle range due to the effect of noninstanton tunneling, while in the limit $\omega \to 0$, it converges on a constant value depending on the strength of perturbation ϵ as well as the input energy E_I, which can be explained by the adiabatic approximation.

However, in the range $\omega > \omega_{cq}$, the tunneling amplitude decays in a little different manner compared with that of the periodically perturbed Eckart barrier. Actually, it exhibits power law decay as $\propto \omega^{-1}$ rather than exponential decay

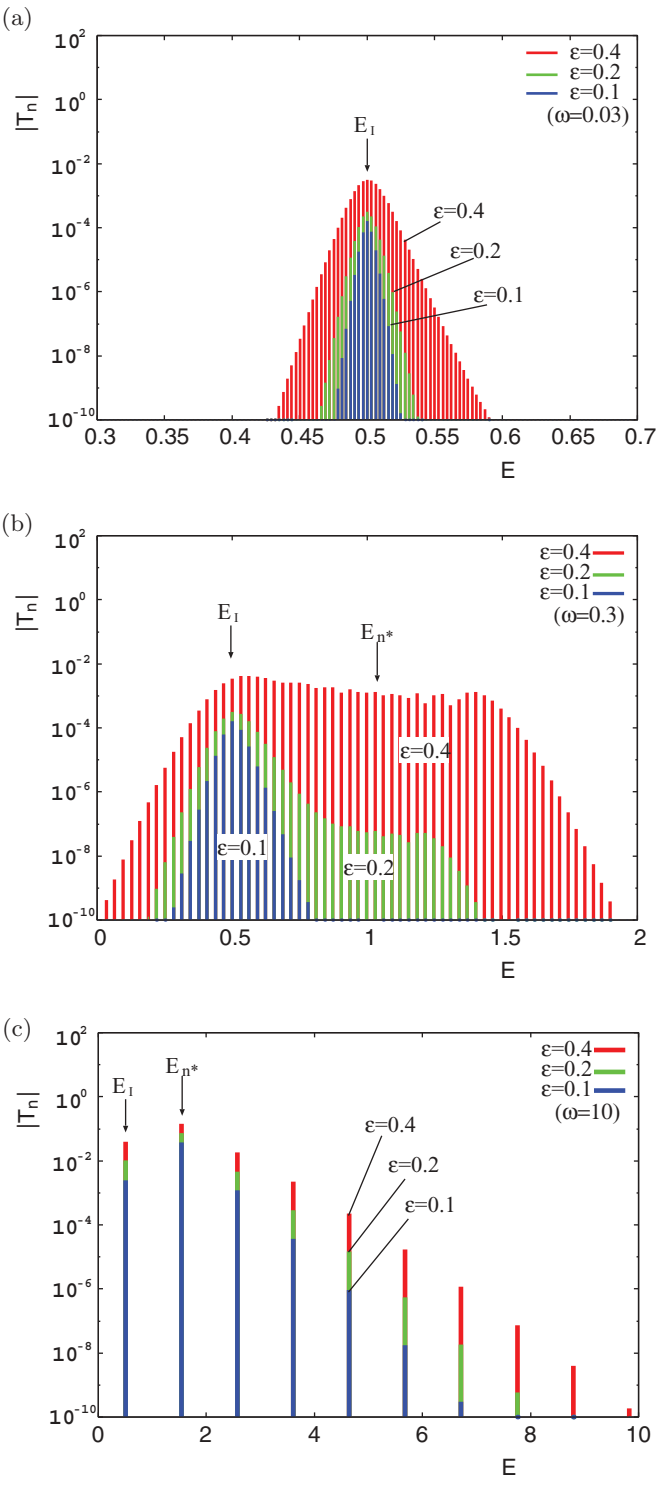

FIG. 4. (Color online) Tunneling spectra of the periodically perturbed rectangular barrier, i.e., $|T_n|$. The width of the potential is taken at $|b_w| = 1$. The input energy E_I and the Planck constant $\hbar$, respectively, take the same values as those of the periodically perturbed Eckart barrier. (a) $\omega = 0.03$. (b) $\omega = 0.3$. (c) $\omega = 10$.

observed for the rounded-off barrier [17]. It is predicted theoretically that the power law decay occurs for excited energy levels in high-frequency ranges [23], and it seems to be the common feature for right-angled potentials. Actually, the

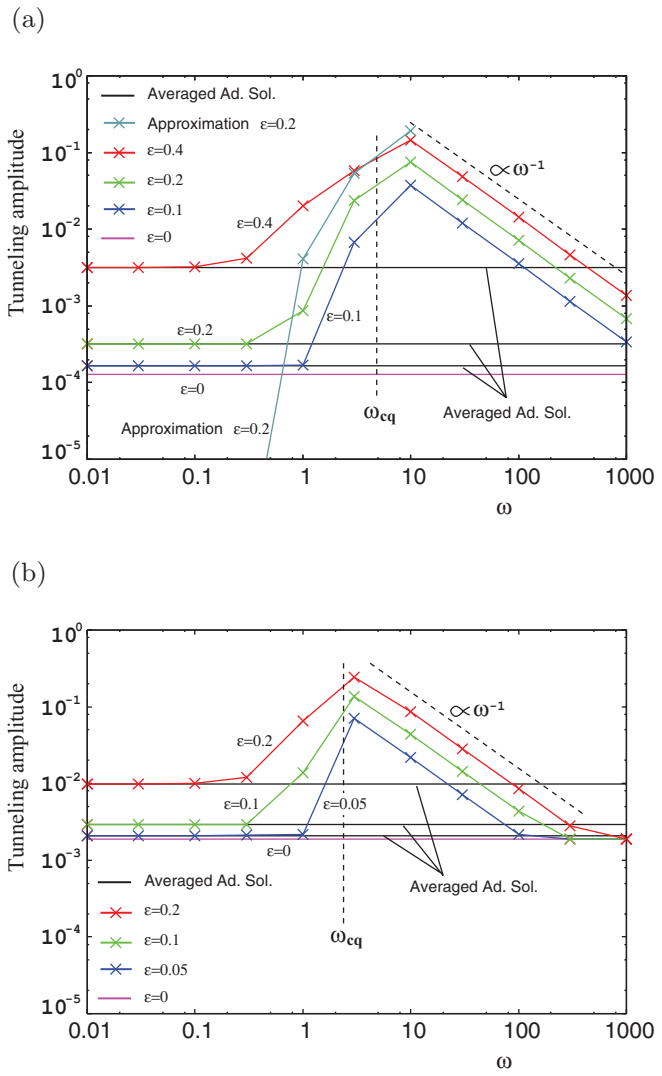

FIG. 5. (Color online) Change of tunneling amplitude (the maximum value of the peaks of the tunneling spectrum) with ω for the periodically perturbed rectangular barrier. The line labeled "Averaged Ad. Sol." is obtained by Eq. (38) with Eqs. (35) and (36), and the line labeled "Approximation $\epsilon = 0.2$" in (a) is given by Eq. (32) at $\epsilon = 0.2$. (a) $E_I = 0.5$. (b) $E_I = 0.75$.

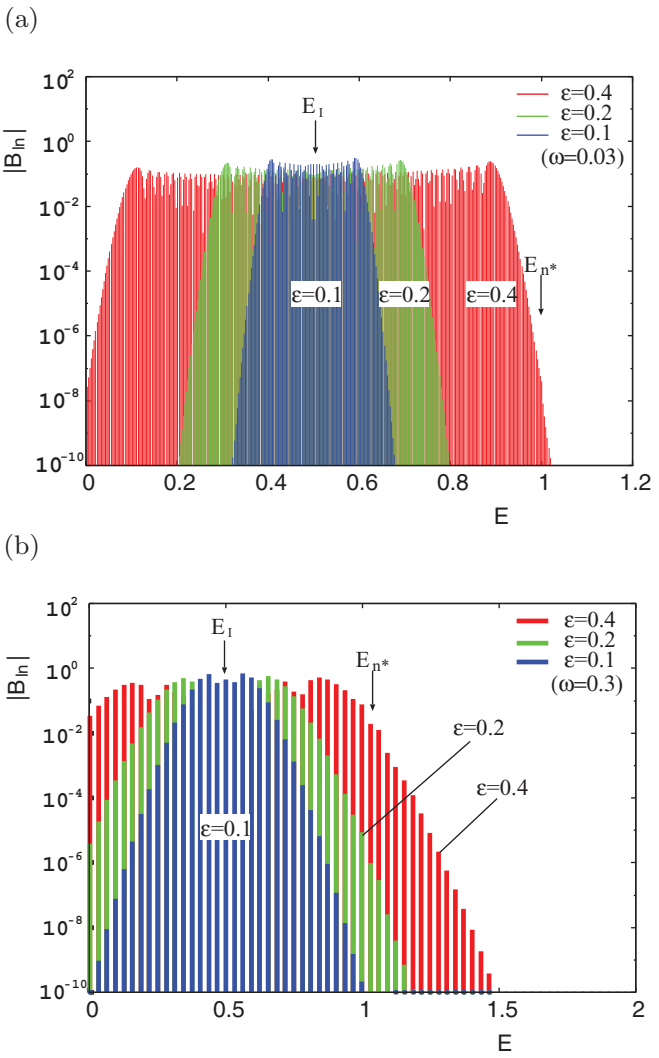

FIG. 6. (Color online) Distributions of $|B_{ln}|$ at $E_I = 0.5$. (a) $\omega = 0.03$. (b) $\omega = 0.3$.

same decay is also observed for the periodically perturbed right-angled step potential [19]. Therefore, the tunneling amplitudes take larger values in some ranges above ω_{cq} for the right-angled potentials compared with the rounded-off potentials. However, since the peaks at the excited energy levels decrease monotonically then the tunneling amplitude converges on the unperturbed solution, namely, the peak at $E = E_I$, in the limit $\omega \to \infty$ independently of ϵ as shown in Fig. 5(b). In Fig. 5(a) they seem to converge on the unperturbed solution, but it occurs out of the numerical range of ω.

C. Approximate solutions for $\omega < \omega_{cq}$

In this subsection we give approximate solutions of noninstanton tunneling and instanton-type tunneling in low and middle frequency ranges. They are used to evaluate the tunneling amplitudes caused by the individual tunneling mechanisms and to judge the winner of the competition between the two mechanisms.

1. Noninstanton tunneling for $E_n > 1$

Let us consider the approximations of the coefficients B_{ln} and B_{rn}. Figure 6(a) and 6(b) show the distributions of $|B_{ln}|$ for $\omega = 0.03$ and 0.3, respectively. The distribution of $|B_{ln}|$ forms a plateau over the range $(E_I - \epsilon < E < E_I + \epsilon)$. The smaller the frequency ω is, the steeper the side cliffs of the plateau become. This fact is the key to understand the tunneling process caused by noninstanton tunneling.

We first consider the approximation of B_{ln}. Equations (17) and (18) are written as

$$\sum_m J_{m-n} X_m(n) = \delta_{n,0}, \tag{21}$$

$$\sum_m J_{m-n} Y_m(n) = 0, \tag{22}$$

where

$$X_m(n) = i^{m-n}[(P_{rn} + P_{bm})B_{lm} + (P_{rn} - P_{bm})B_{rm}]/2P_I, \quad (23)$$

$$Y_m(n) = i^{m-n}\left[(P_{tn} - P_{bm})e^{\frac{i}{\hbar}P_{bm}|b_w|}B_{lm} + (P_{tn} + P_{bm})e^{-\frac{i}{\hbar}P_{bm}|b_w|}B_{rm}\right]. \quad (24)$$

In the case that $P_{rn} \sim P_{tn} \sim P_I$, the dependence of $X_m(n)$ and $Y_m(n)$ on n can be ignored. From analogy to the equality $\sum_m J_{m+n}J_m = \delta_{n,0}$ [31] together with the equality $J_{-n} = (-1)^n J_n$, we can give a plausible assumption that $|X_m(n)|$ is approximated by $|J_m|$ and $Y_m(n) = 0$ as the lowest order approximation. Since the approximation $Y_m(n) = 0$ gives

$$|B_{rn}| \sim \begin{cases} |B_{ln}| \exp\left(-\frac{2}{\hbar}|P_{bn}||b_w|\right), & \text{for } n < n^* \\ |B_{ln}|, & \text{for } n \geqslant n^*, \end{cases} \quad (25)$$

then we can obtain rough estimation that $|B_{ln}| \sim |J_n|$. Although this is very rough estimation, as will be shown below, it actually gives a good approximation even for the case that P_{rn} and P_{tn} are much different from P_I. Note that the same assumption has been successfully applied to the periodically perturbed right-angled step potential in Ref. [19], which corresponds to the case of $B_{rn} = 0$ because of $|b_w| \to \infty$.

In the regime $\hbar\omega \ll \epsilon$, if $|n| \ll \frac{\epsilon}{\hbar\omega}$, $|B_{ln}|$ are estimated using the approximation of the Bessel function [31] as a constant value,

$$|B_{ln}| \sim \left|J_n\left(\frac{\epsilon}{\hbar\omega}\right)\right| \sim \sqrt{\frac{2\hbar\omega}{\pi\epsilon}}, \quad (26)$$

which approximates the height of the plateau over the range $(E_I - \epsilon < E < E_I + \epsilon)$. For $|n| \gg \frac{\epsilon}{\hbar\omega}$, by using the asymptotic form of J_n for large orders $(n \gg 1)$ [31],

$$J_n(x) \sim \sqrt{\frac{1}{2\pi n}}\left(\frac{ex}{2n}\right)^n, \quad (27)$$

we obtain

$$|B_{ln}| \sim \left|J_n\left(\frac{\epsilon}{\hbar\omega}\right)\right| \sim \sqrt{\frac{1}{2\pi n}}\exp\left\{-n\left[\log\left(\frac{2n\hbar\omega}{\epsilon}\right) - 1\right]\right\}, \quad (28)$$

which reproduces the side cliffs of the plateau. Therefore, $|B_{ln}|$ decays more than exponentially with $|n|$, because $\log(\frac{2n\hbar\omega}{\epsilon}) - 1 > 0$, if $|n| > \frac{e}{2}\frac{\epsilon}{\hbar\omega} > \frac{\epsilon}{\hbar\omega}$.

In Fig. 7(a) and 7(b), the approximations of $|B_{ln}|$ and $|B_{rn}|$ given by Eqs. (26), (28), and (25) are compared with the numerical results at $\omega = 0.03$ and 0.3 and at $\epsilon = 0.2$. At the relatively larger frequency $\omega = 0.3$, the approximations are in good agreement with the numerical results for both $|B_{ln}|$ and $|B_{rn}|$. At the smaller frequency $\omega = 0.03$, the approximations well reproduce the plateaus but overestimate the cliff parts. This is mainly because the lowest asymptotic form of $J_n(x)$ for large orders $(n \gg 1)$ (27) does not provide a good approximation for large values of x, namely, $\frac{\epsilon}{\hbar\omega}$ should not be extremely large. However, the approximation $|B_{ln}| \sim |J_n|$ without using the asymptotic form (27) gives a better result, though we do not show it.

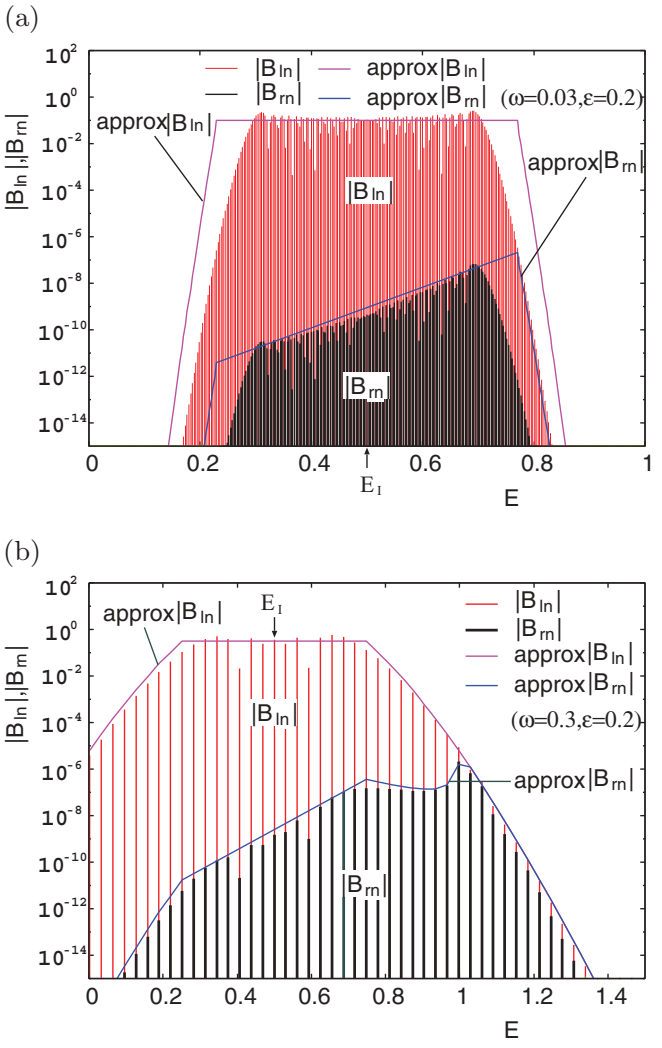

FIG. 7. (Color online) Comparison of $|B_{ln}|$ and $|B_{rn}|$ with the approximate solutions at $\epsilon = 0.2$. The lines labeled "approx $|B_{ln}|$" and "approx $|B_{rn}|$" are, respectively, the results of the approximations of $|B_{ln}|$ and $|B_{rn}|$ obtained by Eqs. (26), (28), and (25). (a) $\omega = 0.03$. (b) $\omega = 0.3$.

Noninstanton tunneling is caused by the wave components which go over (and are just below) the oscillating top of the barrier. From Eq. (25), the magnitude of the terms in the inner parentheses in the right-hand side of Eq. (20), i.e., $e^{\frac{i}{\hbar}P_{bm}|b_w|}B_{lm} + e^{-\frac{i}{\hbar}P_{bm}|b_w|}B_{rm}$, is roughly evaluated as $|B_{lm}|$ for $m \geqslant n^*$. Then, from Eq. (28), it decays more than exponentially with m. For $m < n^*$, P_{bm} takes an imaginary value, then from Eq. (25), it is roughly estimated as

$$\exp\left(-\frac{1}{\hbar}|P_{bm}||b_w|\right)|B_{lm}| \sim \exp\left(-\frac{1}{\hbar}|b_w|\sqrt{2\hbar\omega\Delta m}\right)|B_{lm}|, \quad (29)$$

where $\Delta m \equiv n^* - m$. It is, from Eqs. (26) and (28), true that $|B_{lm}|$ increases with Δm, i.e., with decrease of m, until it reaches the value $\sqrt{\frac{2\hbar\omega}{\pi\epsilon}}$, but it is shown from a more detailed analysis that Eq. (29) decays with Δm, if $\omega|b_w|$ is large enough, because the decay due to the barrier penetration, $\exp(-\frac{1}{\hbar}|P_{bm}||b_w|)$, overwhelms the increase of $|B_{lm}|$. Thus,

the main contribution comes from the threshold component at $m = n^*$ and/or one just below it($m = n^* - 1$), depending on the positions of E_{n^*} and E_{n^*-1} with respect to $E = 1$. Here we roughly estimate it only with the threshold component, since the component at $m = n^* - 1$ makes almost the same contribution, when it is dominant. Then, from Eq. (20), the spectrum $|T_n|$ caused by noninstanton tunneling is estimated as

$$|T_n| \sim \left|J_{n^*-n}\left(\frac{\epsilon}{\hbar\omega}\right)\right||B_{ln^*}| \sim \left|J_{n^*-n}\left(\frac{\epsilon}{\hbar\omega}\right)\right|\left|J_{n^*}\left(\frac{\epsilon}{\hbar\omega}\right)\right|. \tag{30}$$

Applying the asymptotic forms of J_n in Eqs. (26) and (28) to $J_{n^*-n}(\frac{\epsilon}{\hbar\omega})$ in Eq. (30), one can see that the spectrum $|T_n|$ forms a plateau over the range $(E_{n^*} - \epsilon < E < E_{n^*} + \epsilon)$. Since $|B_{ln}|$ at $n = n^*$ is estimated as

$$\begin{aligned}|B_{ln^*}| &\sim \left|J_{n^*}\left(\frac{\epsilon}{\hbar\omega}\right)\right| \\ &\sim \sqrt{\frac{1}{2\pi n^*}}\exp\left\{-n^*\left[\log\left(\frac{2n^*\hbar\omega}{\epsilon}\right)-1\right]\right\} \\ &\sim \sqrt{\frac{\hbar\omega}{2\pi(1-E_I)}} \\ &\quad\times\exp\left(-\frac{1-E_I}{\hbar\omega}\left\{\log\left[\frac{2(1-E_I)}{\epsilon}\right]-1\right\}\right),\end{aligned} \tag{31}$$

where the approximation $n^*\hbar\omega \sim 1 - E_I$ is made use of in the last line, then the height of the plateau spectrum is estimated as

$$\begin{aligned}|T_{n^*}| &\sim \sqrt{\frac{2\hbar\omega}{\pi\epsilon}}|B_{ln^*}| \\ &\sim \frac{\hbar\omega}{\pi\sqrt{\epsilon(1-E_I)}} \\ &\quad\times\exp\left(-\frac{1-E_I}{\hbar\omega}\left\{\log\left[\frac{2(1-E_I)}{\epsilon}\right]-1\right\}\right),\end{aligned} \tag{32}$$

which is mainly determined by $|B_{ln^*}|$.

By using the approximation

$$T_n \sim C\mathrm{e}^{-\frac{i}{\hbar}P_{ln}|b_w|}i^{n^*-n}J_{n^*-n}, \tag{33}$$

where $|C| \sim |B_{ln^*}|$, and Eq. (16) in Eq. (7), we get

$$\begin{aligned}\Psi_T(Q = b_w, t) &= \sum_n T_n\mathrm{e}^{-\frac{i}{\hbar}(P_{ln}b_w + E_n t)} \\ &\sim C\mathrm{e}^{\frac{i}{\hbar}(\frac{\epsilon}{\omega}\cos\omega t - E_{n^*}t)},\end{aligned} \tag{34}$$

which means that the plateau spectrum is caused by the modulation $\mathrm{e}^{\frac{i}{\hbar}\frac{\epsilon}{\omega}\cos\omega t}$ due to the oscillation of the potential. In the case that the semiclassical analysis based on SUMGT is applied to the periodically perturbed rounded-off barrier, the oscillation of the potential induces the oscillation of the unstable manifold over the range $(1 - \epsilon < E < 1 + \epsilon)$, which forms the main body of the plateau spectrum [14,15].

A similar plateau spectrum caused by noninstanton tunneling is also observed for the periodically perturbed right-angled step potential, and it is evaluated by essentially the same approximation [19]. As pointed out in Ref. [19], noninstanton tunneling observed for $\omega < \omega_{cq}$ is attributed to the multiple absorption of quanta induced by the periodical perturbation, which should occur for any periodically perturbed barriers and step potentials. In the limit $\omega \to 0$, the number of quanta absolved in the tunneling process becomes infinity, and the tunneling probability caused by noninstanton tunneling decays exponentially as predicted by Eq. (32) [19]. Actually, as shown in Fig. 5(a), the prediction given by Eq. (32) at $\epsilon = 0.2$ well follows the change of the tunneling amplitude obtained numerically in the range $(1 \leqslant \omega \leqslant 10)$, although the prediction rather overestimates in magnitude. The reason of the overestimation will be discussed later.

2. *Fourier decomposition of adiabatic solution for $E_n < 1$*

The approximations (26), (28), and (25) cannot be used in Eq. (20) to reproduce the localized spectrum caused by instanton-type tunneling (barrier penetrating tunneling), because they ignore the phases of B_{ln} and B_{rn}. Since their major parts widely spread over the energy range $(E_I - \epsilon < E_n < E_I + \epsilon)$, phase cancellation among the terms in Eq. (20) is necessary to form a localized spectrum. But it is not easy to evaluate the summation in Eq. (20) taking into account the phase information of B_{ln} and B_{rn}. Instead, we here use an adiabatic approximation based on the solution of the unperturbed system (see Appendix A), because it is confirmed that it works well in the low-frequency regime [17].

In the adiabatic approximation, P_b is approximated by

$$\tilde{P}_b(t) = i\sqrt{2[a(t) - E_I]}, \tag{35}$$

where $a(t) = 1 + \epsilon\sin\omega t$ is the instantaneous height of the potential. The instantaneous transmissive coefficient $\tilde{T}(t)$ is given by

$$\tilde{T}(t) = \mathrm{e}^{-\frac{i}{\hbar}P_I|b_w|}\left[\mathrm{e}^{-\frac{1}{\hbar}|\tilde{P}_b(t)||b_w|}\tilde{B}_l(t) + \mathrm{e}^{\frac{1}{\hbar}|\tilde{P}_b(t)||b_w|}\tilde{B}_r(t)\right] \tag{36}$$

$$\sim \mathrm{e}^{-\frac{i}{\hbar}P_I|b_w|}\mathrm{e}^{-\frac{1}{\hbar}|\tilde{P}_b(t)||b_w|}\frac{4P_I\tilde{P}_b(t)}{[P_I + \tilde{P}_b(t)]^2}, \tag{37}$$

where the instantaneous values of the coefficients $\tilde{B}_l(t)$ and $\tilde{B}_r(t)$ are obtained by substituting $\tilde{P}_b(t)$ into the place of P_b in Eqs. (A13) and (A10), respectively.

The averaged weight over the period of the perturbation is given by

$$T_0 \sim \langle\tilde{T}(t)\rangle = \frac{1}{T}\int_0^T \tilde{T}(t)\,dt, \tag{38}$$

where $T = \frac{2\pi}{\omega}$, and T_n is obtained by using the Fourier decomposition,

$$T_n \sim \frac{1}{T}\int_0^T \tilde{T}(t)e^{in\omega t}\,dt. \tag{39}$$

Since $\tilde{P}_b(t)$ as well as $\tilde{T}(t)$ is a function of ωt, then the change of variable from t to $\tau = \omega t$ in the integrals in Eqs. (38) and (39) shows that T_0 and T_n are independent of ω. But the width of the spectrum envelope changes proportionally to ω, because the interval between the nearest peaks is $\hbar\omega$.

Let us assume that $\epsilon \ll 1 - E_I$ and $\epsilon \sim$ (or $\ll$)$\hbar \ll 1$. The expansion of $\tilde{P}_b$ in powers of ϵ is given by

$$\tilde{P}_b(t) = i\sqrt{2(1-E_I)}\sqrt{1+\frac{\epsilon}{1-E_I}\sin\omega t} \tag{40}$$

$$\sim i\sqrt{2(1-E_I)}\left[1+\frac{1}{2}\frac{\epsilon}{1-E_I}\sin\omega t + \sum_{m=2}^{\infty}(-1)^{m-1}\frac{(2m-3)!!}{m!2^m}\frac{\epsilon^m}{(1-E_I)^m}\sin^m\omega t\right]$$

$$\sim i\sqrt{2(1-E_I)}\left(1+\frac{1}{2}\frac{\epsilon}{1-E_I}\sin\omega t\right). \tag{41}$$

Then $e^{-\frac{1}{\hbar}|\tilde{P}_b(t)||b_w|}$ is estimated as

$$e^{-\frac{1}{\hbar}|\tilde{P}_b(t)||b_w|} \sim e^{-\frac{|b_w|}{\hbar}\sqrt{2(1-E_I)}}O(e^{\pm|b_w|\epsilon^2/(1-E_I)^{3/2}\hbar}) \times\sum_{m=0}^{\infty}\frac{1}{m!}\left[-\frac{\epsilon|b_w|}{\hbar\sqrt{2(1-E_I)}}\right]^m\left(\frac{e^{i\omega t}-e^{-i\omega t}}{2i}\right)^m. \tag{42}$$

We hereafter take $O(e^{\pm|b_w|\epsilon^2/(1-E_I)^{3/2}\hbar}) \sim O(1)$ because of $\epsilon^2/\hbar \ll \epsilon^2/\hbar^2 \sim$ (or $\ll$)$O(1)$ from the assumption.

The constant term in Eq. (42) is estimated as

$$e^{-\frac{|b_w|}{\hbar}\sqrt{2(1-E_I)}}\sum_{m=0}^{\infty}\frac{1}{m!m!}\left[\frac{\epsilon|b_w|}{2\hbar\sqrt{2(1-E_I)}}\right]^{2m} \sim e^{-\frac{|b_w|}{\hbar}\sqrt{2(1-E_I)}}\left[1+\frac{\epsilon^2|b_w|^2}{8\hbar^2(1-E_I)}\right]. \tag{43}$$

Then $\langle\tilde{T}(t)\rangle$ is approximated by

$$\langle\tilde{T}(t)\rangle \sim e^{-\frac{i}{\hbar}P_I|b_w|}\frac{4P_IP_b}{(P_I+P_b)^2}e^{-\frac{|b_w|}{\hbar}\sqrt{2(1-E_I)}} \times\left[1+\frac{\epsilon^2|b_w|^2}{8\hbar^2(1-E_I)}\right]. \tag{44}$$

The term of $e^{-in\omega t}(n>0)$ in Eq. (42) is evaluated as

$$e^{-\frac{|b_w|}{\hbar}\sqrt{2(1-E_I)}}e^{-in\omega t} \times\left\{\sum_{l=0}^{\infty}\frac{1}{(n+l)!l!}(-1)^{n+l}\left[-\frac{\epsilon|b_w|}{2i\hbar\sqrt{2(1-E_I)}}\right]^{n+2l}\right\}. \tag{45}$$

If $|\epsilon|b_w|/(2\hbar\sqrt{2(1-E_I)})|$ is not larger than one, it is further approximated as

$$e^{-\frac{|b_w|}{\hbar}\sqrt{2(1-E_I)}}\frac{1}{n!}\left[\frac{\epsilon|b_w|}{2i\hbar\sqrt{2(1-E_I)}}\right]^n e^{-in\omega t}. \tag{46}$$

Then $T_n(n>0)$ is estimated as

$$T_n \sim e^{-\frac{i}{\hbar}P_I|b_w|}\frac{4P_IP_b}{(P_I+P_b)^2}e^{-\frac{|b_w|}{\hbar}\sqrt{2(1-E_I)}}\frac{1}{n!}\left[\frac{\epsilon|b_w|}{2i\hbar\sqrt{2(1-E_I)}}\right]^n \tag{47}$$

and $|T_{-n}| \sim |T_n|$ from the approximation (42). It means that $|T_n|$ decays with $|n|$ as $|T_n/T_0| \sim O(1/|n|!)$.

Figure 8 shows the comparison of tunneling spectra obtained numerically with those given by the adiabatic solution (39) with Eqs. (35) and (36) at $\epsilon = 0.2$ and at three values of ω, $\omega = 0.01$, 0.03, and 0.1. The numerical results

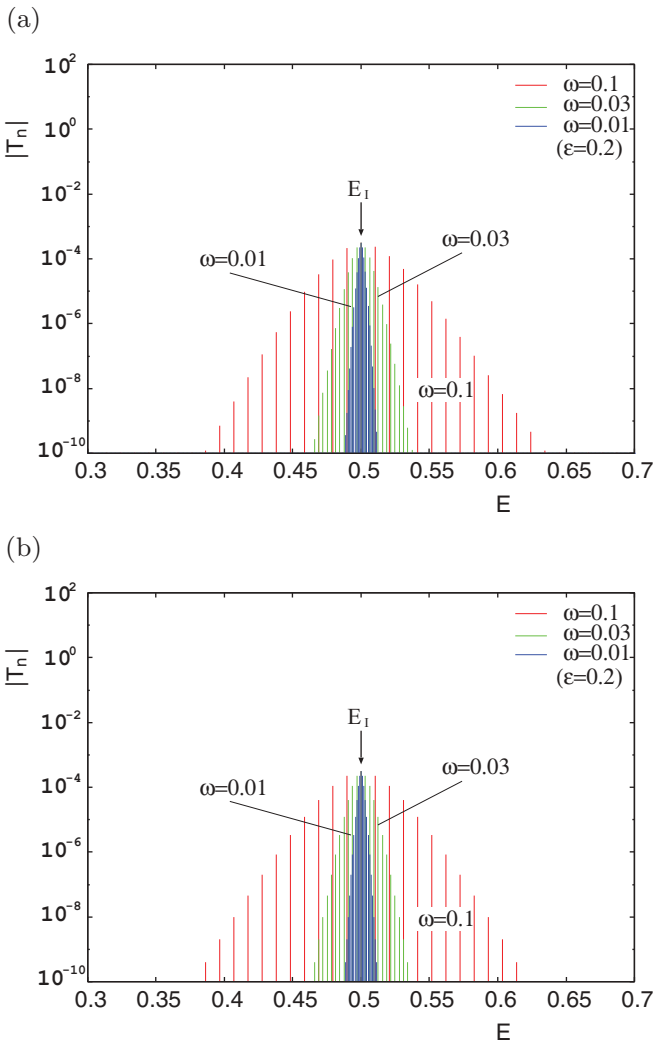

FIG. 8. (Color online) Comparison of tunneling spectra in the low-frequency regime with those obtained by the adiabatic solution. (a) Tunneling spectra at $\epsilon = 0.2$ for $\omega = 0.01$, 0.03, 0.1. (b) Corresponding spectra obtained by the adiabatic solution (39) with Eqs. (35) and (36).

in Fig. 8(a) are well reproduced by the adiabatic solutions in Fig. 8(b), namely, the maximum of the spectrum $|T_0|$ almost agrees with the averaged adiabatic weight (38), which means that in the limit $\omega \to 0$, the tunneling amplitude converges on the averaged weight estimated as "unperturbed weight" $\times[1 + O(\epsilon^2/\hbar^2)]$ in Eq. (44) rather than the maximum instantaneous weight, "unperturbed weight" $\times[1 + O(\epsilon/\hbar)]$, which is larger than it. Furthermore, for all the spectra obtained numerically, the peaks $|T_n|$ at the same n take almost the same value independently of ω, and they decrease as $1/|n|!$ with $|n|$ as shown by Eq. (47). Therefore there is a scaling law in the limit $\omega \to 0$ with respect to the width of the spectrum envelope, namely, it is proportional to $\hbar\omega$.

3. *Overview of the approximate solutions for $\omega < \omega_{cq}$*

In Fig. 9 we compare the tunneling spectra obtained numerically with the approximation solution for noninstanton tunneling (multiphoton-assisted tunneling) and with the adiabatic solution for instanton-type tunneling(barrier penetration).

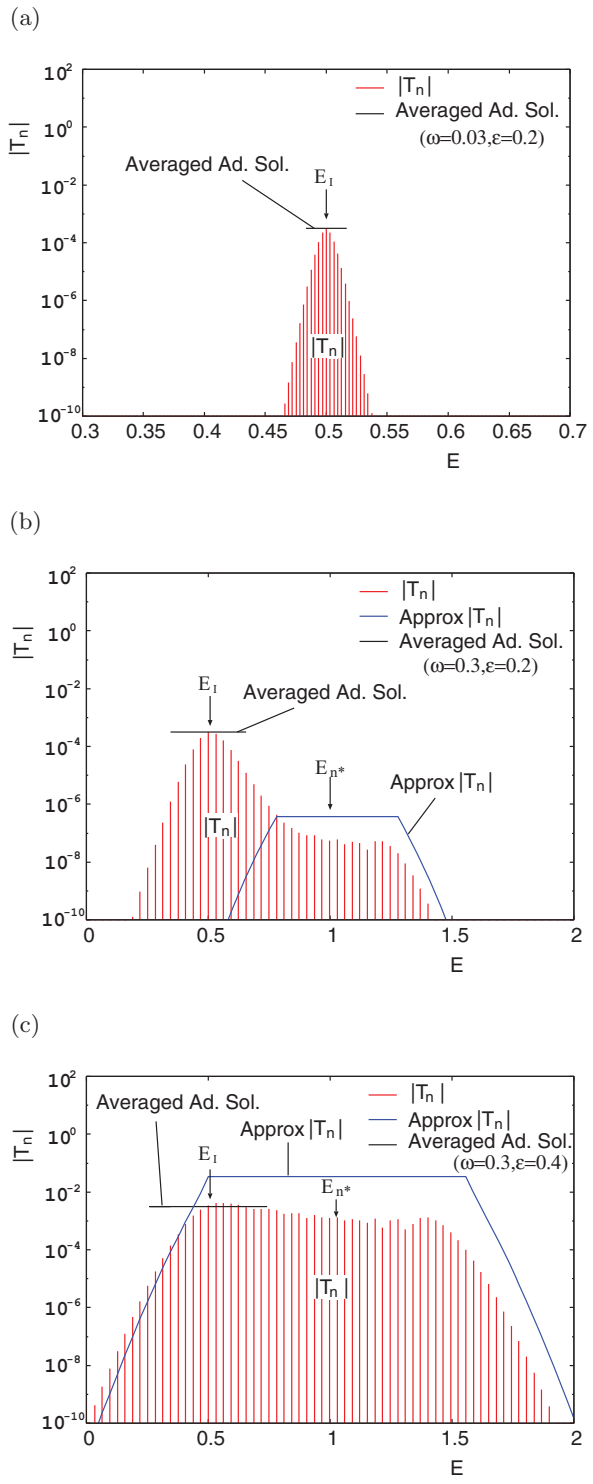

FIG. 9. (Color online) Comparison of tunneling spectra obtained numerically with the approximate solution for noninstanton tunneling and with the adiabatic solution for instanton-type tunneling. The line labeled "Approx $|T_n|$" denotes the approximate solution of the plateau spectrum given by Eq. (30). The line labeled "Averaged Ad. Sol." indicates the averaged adiabatic weight given by Eq. (38) with Eqs. (35) and (36), and it is drawn in the range $(E_{-n_{\max}} \leqslant E \leqslant E_{n_{\max}})$, where $n_{\max}$ is defined by $n_{\max} = \max\{n||T_n/T_0| \geqslant 10^{-2}, n > 0\}$ using $|T_n|$ in Eq. (47). (a) The localized spectrum at $\epsilon = 0.2$ and $\omega = 0.03$. (b) The mixed spectrum at $\epsilon = 0.2$ and $\omega = 0.3$. (c) The plateau spectrum at $\epsilon = 0.4$ and $\omega = 0.3$.

As shown in Fig. 9(a) and 9(b), the averaged adiabatic weight denoted by the line labeled "Averaged Ad. Sol.," which is obtained by Eq. (38) with Eqs. (35) and (36), well approximates the height of the localized spectrum in (a) as well as the height of the head lobe of the mixed spectrum in (b). The line is drawn in the range $(E_{-n_{\max}} \leqslant E \leqslant E_{n_{\max}})$, where $n_{\max}$ is defined by $n_{\max} = \max\{n||T_n/T_0| \geqslant 10^{-2}, n > 0\}$ using $|T_n|$ in Eq. (47), and it well approximates the width of the localized spectrum in Fig. 9(a) and that of the head lobe in Fig. 9(b). These results together with those in Fig. 8 indicate that the adiabatic solution provides a good approximation to instanton-type tunneling.

The line labeled "Approx $|T_n|$" denotes the approximate solution of the plateau spectrum given by Eq. (30). It shows good agreement in shape with the plateau spectrum in Fig. 9(c) as well as the side shoulder of the mixed spectrum in Fig. 9(b), though it overestimates them in height. The overestimation is also confirmed in Fig. 5 (a). Indeed, the line labeled "Approximation $\epsilon = 0.2$," obtained by Eq. (38) with Eqs. (35) and (36) well follows the numerical result at $\epsilon = 0.2$ in a certain range, but it always takes larger values than the numerical result. The fact that the plateau and the side shoulder are smaller in height than the approximate solutions is attributed to destructive interference among the terms of B_{lm} and B_{rm} at $m = n^*$ (dominant) and $m = n^* \pm 1$ (second dominant) in Eq. (20). Note that for the case of the periodically perturbed right-angled step potential which corresponds to the case of $B_{rm} = 0$ and for which the terms for $m < n^*$ are substantially zero, the same approximation is in very good agreement in height as well as in shape with the plateau spectrum obtained numerically [19].

As a result, judging the winner of the competition between the two characteristic tunneling mechanisms, the instanton and noninstanton mechanisms, is simply done by comparison of amplitude between the adiabatic solution of the localized spectrum and the approximate solution of the plateau spectrum. The winner determines the tunneling amplitude, but both tunneling mechanisms contribute to the formation of the entire spectrum, when the contribution of noninstanton tunneling is not much smaller than that of instanton-type tunneling.

D. High-frequency range: $\omega > \omega_{cq}$

In the range $\omega > \omega_{cq}$, the tunneling amplitude is mainly determined by the two components, the fundamental energy level at $n = 0$ and the first excited energy level at $n = 1$. As shown in Appendix B, we take into account only the two levels in calculation of B_{ln}, B_{rn}, R_n, and T_n. As a result, T_0 and T_1 are estimated as

$$T_0 \sim \mathrm{e}^{-\frac{i}{\hbar}P_I|b_w|}\left[\mathrm{e}^{-\frac{1}{\hbar}|P_{b0}||b_w|}\frac{4iP_I|P_{b0}|}{(P_I+i|P_{b0}|)^2} + \left(\frac{\epsilon}{2\hbar\omega}\right)^2 \mathrm{e}^{\frac{i}{\hbar}P_{b1}|b_w|} 2P_I f(E_I)\right] \tag{48}$$

and

$$T_1 \sim -i\mathrm{e}^{-\frac{i}{\hbar}(P_{t1}-P_{b1})|b_w|}\frac{2\epsilon}{\hbar\omega}P_I P_{b1} g(E_I) \sim O\left(\frac{\epsilon}{\hbar\omega}\right), \tag{49}$$

where $f(E_I) = \tilde{f}(P_I(E_I), P_{b0}(E_I), P_{b1}(E_I), P_{t1}(E_I))$ and $g(E_I) = \tilde{g}(P_I(E_I), P_{b0}(E_I), P_{b1}(E_I), P_{t1}(E_I))$ are functions of

$O(1)$. In the limit $\omega \to \infty$, T_0 converges on the unperturbed solution [see Eq. (A14)], while T_1 decays as $\propto 1/\omega$. The power law decay of the first excited state ($\propto 1/\omega$) (or the decay of tunneling probability as $\propto 1/\omega^2$) seems to be the common feature in the high-frequency range for periodically perturbed right-angled potentials, i.e., rectangular barrier, step and so on, although an exponential decay is observed for periodically perturbed rounded-off potentials [17,19].

In the range ($\omega_{cq} < \omega < \frac{\epsilon}{\hbar} e^{\frac{1}{\hbar}|P_{b0}||b_w|}$), the relation $|T_1| > |T_0|$ is satisfied, and the first excited state dominates the tunneling process. But the unperturbed instanton becomes dominant, when ω goes beyond this range, namely, $\omega > \frac{\epsilon}{\hbar} e^{\frac{1}{\hbar}|P_{b0}||b_w|}$ and $|T_1| < |T_0| (\sim e^{-\frac{1}{\hbar}|P_{b0}||b_w|})$. This change of the tunneling amplitude is actually seen in Fig. 5(b).

IV. CORRESPONDENCE BETWEEN THE SEMICLASSICAL AND QUANTUM INTERPRETATIONS

In this section we discuss the tunneling features of the periodically perturbed Eckart barrier, which can be reproduced in the low and middle frequency ranges by the complex semiclassical method, and we discuss the correspondence between the semiclassical interpretation for the Eckart barrier and the quantum interpretation for the rectangular barrier.

A. Semiclassical formula

The semiclassical S matrix for periodically perturbed scattering potentials is given by [29,32]

$$S(E_O,E_I) \sim \lim_{|Q_I|,|Q_O|\to\infty} \sum_{\text{c.t.}} \frac{\sqrt{|P_I||P_O|}}{\sqrt{2\pi i\hbar P_I P_O}} \sqrt{-\frac{\partial^2 S_S}{\partial E_I \partial E_O}} \times e^{-i(P_O Q_O - P_I Q_I)/\hbar} e^{\frac{i}{\hbar} S_S(Q_O,E_O,Q_I,E_I)}, \quad (50)$$

where the classical action is defined by

$$S_S = \int_{Q_I}^{Q_O} P\, dQ - \int_{t_I}^{t_O} H(Q,P,\omega t)\, dt + E_O t_O - E_I t_I. \quad (51)$$

The summation $\sum_{\text{c.t.}}$ is taken over all the contributing (complex) trajectories satisfying the input and output boundary conditions, which are, respectively, given by [29,32]

$$\mathcal{I} = \{(t_I,Q,P)|t_I \in \mathbf{C}, \quad Q = Q_I, \quad P = P_I(=-\sqrt{2E_I})\} \quad (52)$$

and

$$\mathcal{F} = \{(t_O,Q,P)|t_O \in \mathbf{C}, \quad Q = Q_O, \quad P = P_O(=-\sqrt{2E_O})\}. \quad (53)$$

Due to the periodicity of the system, the initial points of the contributing trajectories appear periodically with the period $T(=2\pi/\omega)$ in the initial plane $\mathcal{I}$. Then it is possible to reproduce the quantum probability by using the trajectories whose initial points are in a unit interval. To do this, the semiclassical S matrix is rewritten as [32]

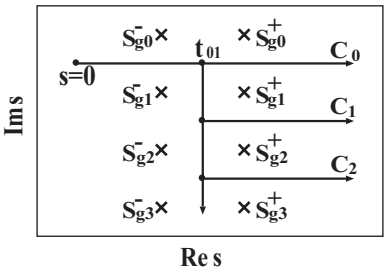

FIG. 10. Singularities and representative integration paths on the lapse time plane.

$$S(E_O,E_I) \sim \lim_{|Q_I|,|Q_O|\to\infty} \sum_n \hbar\omega\delta(E_O - E_I - n\hbar\omega) \times \sum_{\text{c.t.}\in\mathcal{I}^*} \frac{1}{\sqrt{2\pi i\hbar}} \frac{\sqrt{|P_I||P_O|}}{\sqrt{P_I P_O}} \sqrt{-\frac{\partial^2 S_S}{\partial E_I \partial E_O}} \times e^{-i(P_O Q_O - P_I Q_I)/\hbar} e^{iS_S(Q_O,E_O,Q_I,E_I)/\hbar}, \quad (54)$$

where $\mathcal{I}^* = \{t_I | -T < \text{Re}t_I \leqslant 0\}$ denotes a unit of $\mathcal{I}$. The periodicity creates comb spikes with the interval $\hbar\omega$, which is represented as $\sum_n \hbar\omega\delta(E_O - E_I - n\hbar\omega)$. In numerical calculation, $\delta(E_O - E_I - n\hbar\omega)$ is, for normalization, replaced by $\delta_{n,(E_O-E_I)/\hbar\omega}$.

B. Unperturbed solution and instanton-type tunneling

The classical solution for the unperturbed system is given by [29]

$$Q(t) = \sinh^{-1}\{\lambda \cosh[\sqrt{2E_I}(t - t_0)]\}, \quad (55)$$

where $\lambda \equiv \sqrt{1/E_I - 1}$ and t_0 is the time at which the trajectory hits the turning point [29,32]. Giving an initial condition [$Q = Q_I(\gg 1), P = P_I(=-\sqrt{2E_I} < 0)$] at $t = t_I$, the interval between t_0 and t_I is determined by $t_0 - t_I = (Q_I - \log\lambda)/\sqrt{2E_I} \equiv t_{01}$.

As shown in Fig. 10, the solution has singularities in the lapse time plane $s = t - t_I$, and the singularities are aligned along two vertical lines, i.e., entrance singularities Sg_n^- and exit singularities Sg_n^+. The distances between the singularities are given as follows: $Sg_n^\pm - Sg_{n+1}^\pm = i\pi/\sqrt{2E_I}$ and $Sg_n^+ - Sg_n^- = 2\frac{1}{\sqrt{2E_I}}\sinh^{-1}(1/\lambda)$.

In Fig. 10 topologically different integration paths used for calculation of complex trajectories are also drawn. The trajectory along the integration path C_1 gives the major contribution to tunneling. The complex trajectory with imaginary time evolution along the vertical part of the path C_1 is called "instanton" [20], and the imaginary depth of the instanton is determined by [16]

$$t_{\text{inst}}(E_I) = -\pi/\sqrt{2E_I}. \quad (56)$$

The tunneling amplitude for the unperturbed system is estimated by using the instanton,

$$W_I = \exp\left(-\frac{1}{\hbar}\text{Im}S_{I0}\right), \quad (57)$$

where $\mathrm{Im}S_{I0}$ denotes the imaginary part of the classical action along the instanton, which is obtained as

$$\mathrm{Im}S_{I0} = \sqrt{2E_I}\,\frac{1-E_I}{E_I+\sqrt{E_I}}. \tag{58}$$

When a small perturbation with $\omega \ll 1$ is applied to the system, a localized tunneling spectrum is observed. It is expected that the topology of integration paths is essentially the same as that of the unperturbed solution [13–15] and that the adiabatic approximation based on the instanton can be applicable. The instantaneous classical action is given by

$$\mathrm{Im}S_I = \sqrt{2E_I}\,\frac{a(t)-E_I}{E_I+\sqrt{a(t)E_I}}, \tag{59}$$

where $a(t) = 1+\epsilon\sin\omega t$ denotes the height of the time dependent barrier. At a glance the effective tunneling weight of instanton seems to be given by $\exp(-\frac{1}{\hbar}\mathrm{Im}S_I)$ at $a(t) = 1-\epsilon$, i.e., the smallest imaginary action during the period of the perturbation. However, the tunneling amplitude is really given by the time average of instantaneous instanton weights [16]:

$$W_{\mathrm{av}} = \frac{1}{T}\int_0^T \exp\left(-\frac{1}{\hbar}\mathrm{Im}S_I\right)\,dt, \tag{60}$$

which is estimated as

$$W_{\mathrm{av}} \sim \exp\left[-\frac{\pi}{\hbar}\sqrt{2}(1-\sqrt{E_I})\right]\left(1+\frac{\epsilon^2\pi^2}{8\hbar^2}\right). \tag{61}$$

The correction in the last parentheses due to the perturbation is of $O(\epsilon^2/\hbar^2)$, which is the same order as that of the periodically perturbed rectangular barrier in Eq. (44). The height of nth spectrum peak is given by

$$W_{\mathrm{av},n} = \frac{1}{T}\int_0^T \exp\left(-\frac{1}{\hbar}\mathrm{Im}S_I\right)\exp(i\omega nt)\,dt, \tag{62}$$

which is estimated for $n > 0$ as

$$W_{\mathrm{av},n} \sim \exp\left[-\frac{\pi}{\hbar}\sqrt{2}(1-\sqrt{E_I})\right]\frac{1}{n!}\left(\frac{\epsilon\pi}{i2\sqrt{2}\hbar}\right)^n, \tag{63}$$

and $|W_{\mathrm{av},-n}| = |W_{\mathrm{av},n}|$. $|W_{av,n}|$ is independent of ω but decreases with $|n|$ as $|W_{\mathrm{av},n}/W_{\mathrm{av}}| \sim O(1/|n|!)$. Therefore, instanton-type tunneling generates essentially the same localized spectrum in the lower-frequency range as that of the periodically perturbed rectangular barrier.

Figure 11 shows the comparison of tunneling spectra at $\epsilon = 0.2$ in the low-frequency regime with the adiabatic instanton spectra obtained by Eqs. (60) and (62). The adiabatic instanton spectra in Fig. 11(b) are almost the same as the tunneling spectra obtained numerically in Fig. 11(a) for $\omega = 0.01$ and 0.03. However, the spectrum obtained numerically at $\omega = 0.1$ more extends to an upper energy range compared with the adiabatic spectrum in Fig. 11(b), while they show good agreement in the lower half, i.e., $E_n < E_I$. Therefore, the spectra of the periodically perturbed rounded-off barrier have the same properties in the limit $\omega \to 0$ as those of the periodically perturbed rectangular barrier, and the same scaling law with respect to the width of the spectrum envelope exists for both systems: the width $\propto \hbar\omega$.

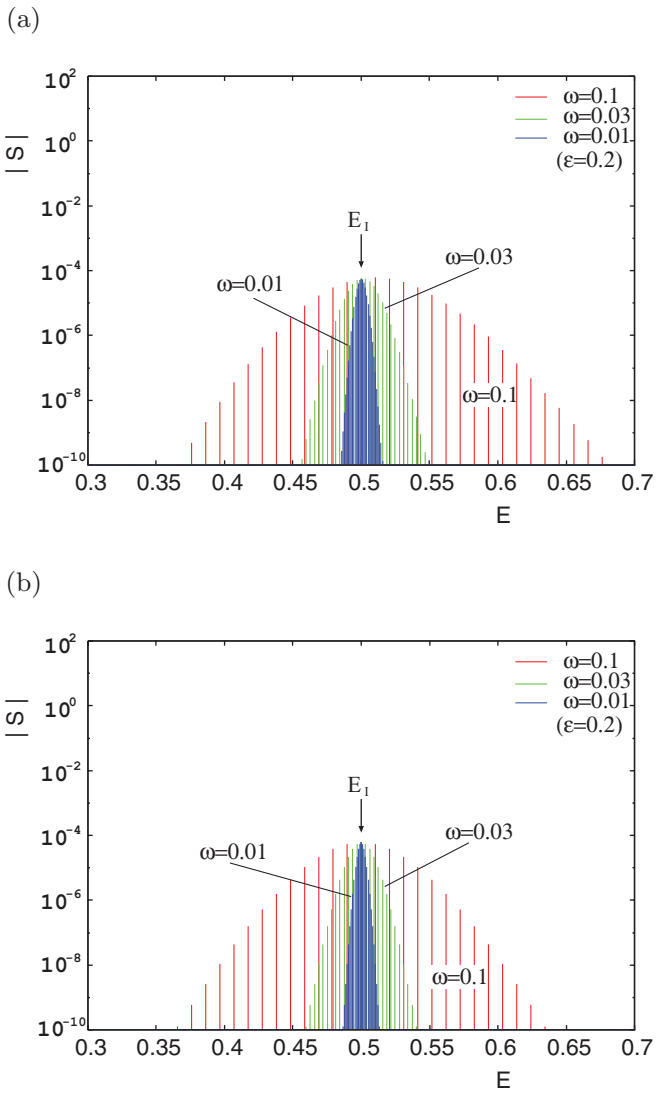

FIG. 11. (Color online) Comparison of tunneling spectra in the low-frequency regime with the spectra obtained by the adiabatic instanton for the periodically perturbed Eckart barrier. (a) Tunneling spectra at $\epsilon = 0.2$ for $\omega = 0.01, 0.03, 0.1$. (b) Corresponding spectra of the adiabatic instanton solution given by Eqs. (60) and (62).

To confirm the reproducibility of the localized spectrum by the complex semiclassical method, we carry out the full complex semiclassical calculation with the semiclassical S matrix (54). Figure 12 shows the semiclassical result at $\epsilon = 0.2$ and $\omega = 0.03$. In Fig. 12(a), the initial set of contributing trajectories C extends to positive and negative imaginary sides compared with the imaginary depth of the unperturbed instanton. This indicates that as the initial point goes to the upper or lower end of the branch C, the imaginary part of the classical action takes larger values, which make extremely smaller contributions to tunneling. In the complex semiclassical theory, the rapidly dropping tails of the spectrum envelope are attributed to the increasing imaginary part of the classical action. The resultant tunneling spectrum in Fig. 12(b) well reproduces the localized spectrum obtained by the quantum calculation in Fig. 11(a).

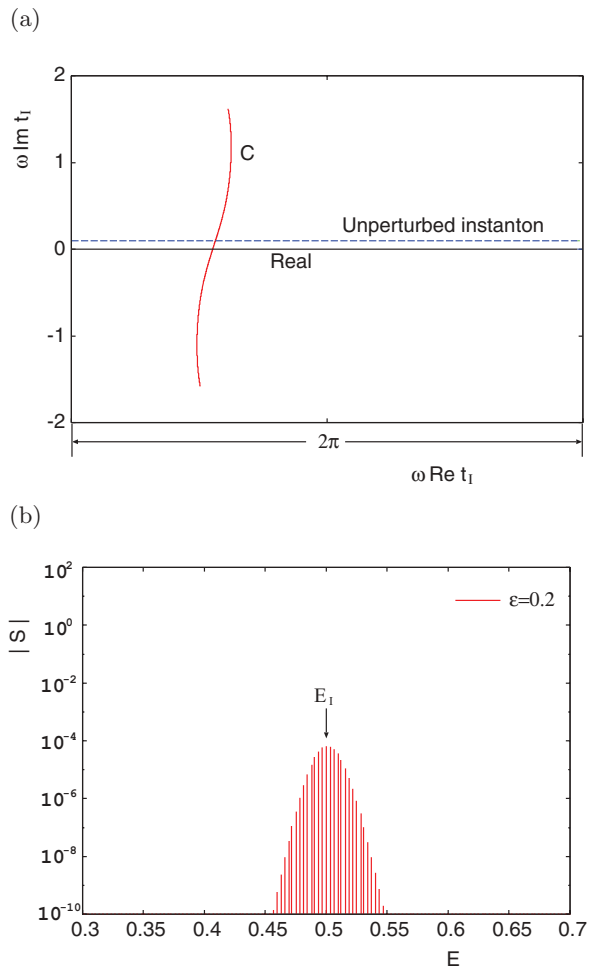

FIG. 12. (Color online) Tunneling spectrum reproduced by the full complex semiclassical calculation at $\epsilon = 0.2$ and $\omega = 0.03$. (a) The set of the initial points of contributing trajectories C on the complex initial time plane. For comparison, the imaginary depth of the unperturbed instanton is drawn. (b) Semiclassical tunneling spectrum.

C. SUMGT weight in low- and middle-frequency ranges

Noninstanton tunneling in the low- and middle-frequency ranges ($\omega < \omega_{cq}$) can be reproduced by the complex semiclassical method. It is explained by stable-unstable manifold guided tunneling (SUMGT) [13–16].

When the classical transportation to the transmissive side is prohibited, namely, the only quantum tunneling contributes to the transportation, the real part of the initial plane $\mathcal{I}$ does not intersect with the stable manifold W_s of the unstable periodic orbit at the top of the barrier. However, as shown in Fig. 13, there always exists in the complex domain the intersection between $\mathcal{I}$ and W_s, which forms isolated points called the critical point t_{Ic}. The SUMGT trajectories are those trajectories which start from a small neighborhood of the critical point, go toward the unstable periodic orbit guided by the complex W_s, and pass close to it. After that, some of SUMGT trajectories go to the transmissive side guided by the complex unstable manifold W_u, thereby contributing to tunneling, though the others guided by the complex W_u in the other side, i.e., the reflective side, contribute to reflection. With the help of the

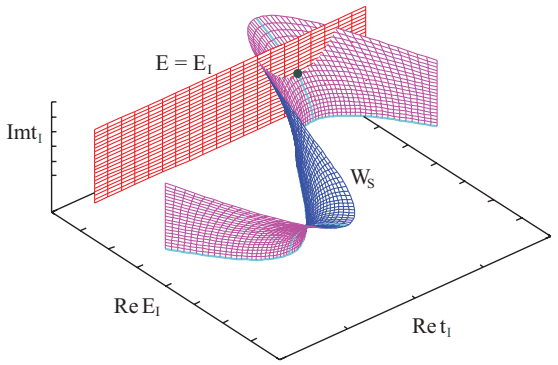

FIG. 13. (Color online) Initial plane at $E = E_I$ and stable manifold W_s in the complex domain. The bullet denotes the intersection between them, i.e., critical point.

Melnikov method [33,34], we can prove the existence of the critical point in the complex domain and evaluate the tunneling probability caused by SUMGT [13–17].

By using the Melnikov method, the imaginary part of the critical point $\mathrm{Im}t_{Ic}$ is estimated as

$$\mathrm{Im}t_{Ic} = \frac{1}{\omega}\cosh^{-1}\left\{\frac{1-E_I}{\epsilon(1-\chi(\omega))}\right\}, \tag{64}$$

where $\chi(\omega)$ is defined by

$$\begin{aligned}\chi(\omega) &\equiv 2\omega\int_0^\infty \frac{\sin\omega s}{1+e^{2\sqrt{2}s}}\,ds \\ &= \omega\left[\frac{1}{\omega} - \frac{\pi}{2\sqrt{2}}\mathrm{cosech}\left(\frac{\omega\pi}{2\sqrt{2}}\right)\right].\end{aligned} \tag{65}$$

In the low-frequency range ($\omega \ll 1$), $\chi(\omega)$ is approximated as $\chi(\omega) \sim \frac{\pi^2}{48}\omega^2$ and $\mathrm{Im}t_{Ic}$ is inversely proportional to ω:

$$\mathrm{Im}t_{Ic} \sim \frac{1}{\omega}\cosh^{-1}[(1-E_I)/\epsilon]. \tag{66}$$

In the range of ω in which the relation $\mathrm{Im}t_{Ic} < |t_{\mathrm{inst}}(E_I)|$ is satisfied, where $|t_{\mathrm{inst}}(E_I)|$ is the imaginary depth of instanton defined by Eq. (56), SUMGT seems to overwhelm instanton-type tunneling. Since $|t_{\mathrm{inst}}(E_I)|$ is independent of ω and $\mathrm{Im}t_{Ic}$ converges on $\frac{\pi}{2\sqrt{2}}(< |t_{\mathrm{inst}}(E_I)|)$ in the limit $\omega \to \infty$, then SUMGT governs the tunneling process in the range $(\omega_{ci} < \omega < \omega_{cq})$, where ω_{ci} is the value of ω at which $\mathrm{Im}t_{Ic} = |t_{\mathrm{inst}}(E_I)|$ [17].

From Eq. (54), the semiclassical weight of the SUMGT trajectory is evaluated as

$$W_S = \frac{\hbar\omega}{\sqrt{2\pi\hbar}}\exp\left(-\frac{1}{\hbar}\mathrm{Im}S_S\right). \tag{67}$$

The imaginary part of the classical action of the SUMGT trajectory $\mathrm{Im}S_S$ is well approximated by that of the critical trajectory that starts at the critical point t_{Ic}. The imaginary part of the classical action of the critical trajectory can be evaluated with the help of the Melnikov method [14–17].

As a result, we obtain the following expression of $\mathrm{Im}S_S$:

$$\mathrm{Im}S_S \sim \mathrm{Im}t_{Ic}(1-E_I) - \frac{1-E_I}{\omega}\tanh(\omega \mathrm{Im}t_{Ic}) + \sqrt{2}\sinh(\omega \mathrm{Im}t_{Ic})\int_{\infty}^{0} dx \int_{\infty}^{x} \mathrm{d}s \frac{\epsilon \sin \omega s}{\cosh^2(\sqrt{2}s)}. \tag{68}$$

Taking into account the fact that the last term in the right-hand side of Eq. (68) take a finite value in the limit $\omega \to 0$ and using Eq. (66), we can estimate $\mathrm{Im}S_S$ in the low-frequency range as

$$\mathrm{Im}S_S \sim \mathrm{Im}t_{Ic}(1-E_I) - \frac{1-E_I}{\omega}\tanh(\omega \mathrm{Im}t_{Ic}) \tag{69}$$

$$\sim \frac{1-E_I}{\omega}\left(\cosh^{-1}\left[\frac{(1-E_I)}{\epsilon}\right] - \tanh\left\{\cosh^{-1}\left[\frac{(1-E_I)}{\epsilon}\right]\right\}\right). \tag{70}$$

For the case that $1-E_I \gg \epsilon$, $\mathrm{Im}S_S$ is further approximated as

$$\mathrm{Im}S_S \sim \frac{1-E_I}{\omega}\{\log[2(1-E_I)/\epsilon] - 1\}, \tag{71}$$

and we obtain

$$W_S \sim \frac{\hbar\omega}{\sqrt{2\pi\hbar}}\exp\left(-\frac{1-E_I}{\hbar\omega}\left\{\log\left[\frac{2(1-E_I)}{\epsilon}\right] - 1\right\}\right). \tag{72}$$

Equation (72) is very similar to the approximate amplitude of multiphoton-assisted tunneling for the periodically perturbed rectangular barrier in Eq. (32). Especially the arguments of the exponential functions coincide with each other. Therefore, the noninstanton tunneling induced by SUMGT for the periodically perturbed rounded-off barrier has the same characteristic in the range ($\omega < \omega_{cq}$) as multiphoton-assisted tunneling for the periodically perturbed rectangular barrier. However, they exhibit different characteristics for $\omega > \omega_{cq}$. Namely, the exponential decay is observed for the periodically perturbed rounded-off barrier, but the power law decay occurs for the periodically perturbed rectangular barrier [17,19].

In Fig. 2, the line labeled "SUMGT" is the result of Eq. (67) with Eq. (69) and those labeled "Instanton" and "Averaged instanton" are given by Eq. (57) with Eq. (58) and Eq. (60) with Eq. (59), respectively. Near the intersection between the SUMGT weight and the averaged instanton W_{av}, they well capture the transition from instanton-type tunneling to noninstanton tunneling at each value of ϵ. However the SUMGT weight overestimates the tunneling amplitude near ω_{cq} due to the ignorance of the last term in Eq. (68). Actually the calculation using Eq. (68) shows better agreement with it as shown in Refs. [16,17].

V. DISCUSSION

In this paper we have studied tunneling for the periodically perturbed barriers, especially in the low- and middle-frequency ranges, in order to comprehensively understand noninstanton tunneling compared with instanton-type tunneling from the quantum and semiclassical viewpoints. The periodically perturbed rectangular barrier, for which we can handle the exact form of the quantum solution, is used for the purely quantum analysis, while the periodically perturbed Eckart barrier is appropriate for the semiclassical analysis. Very similar tunneling phenomena are observed for both systems through the whole range of perturbation frequency. Especially similar transitions between noninstanton tunneling and instanton-type tunneling are observed with change of the perturbation frequency.

In the low- and middle-frequency ranges ($\omega < \omega_{cq}$), noninstanton tunneling is interpreted as stable-unstable manifold guided tunneling (SUMGT) from the semiclassical viewpoint. Actually, the critical trajectory starting at the critical point t_{Ic} on the complex stable manifold guides the SUMGT trajectories, and the tunneling amplitude is estimated by the imaginary part of the classical action of the critical trajectory. From the quantum viewpoint, it is regarded as multiphoton-assisted tunneling, which makes large jumps of energy absorbing a lot of quanta from the input energy to excited energy levels above the barrier. The tunneling amplitude can be estimated by the coefficient B_{ln} (or B_{rn}) at $n = n^*$, namely at the threshold energy level $E_{n^*} = E_I + n^*\hbar\omega$ [see Eq. (32)]. B_{ln} (or B_{rn}) is the coefficient of the left (or right) -going wave component in the interaction region ($-|b_w| < Q < 0$) and gives the transition rate from the input energy E_I to the energy level E_n. The set of coefficients $|B_{ln}|$ forms the plateau distribution whose flat top spreads over the range ($E - \epsilon < E < E_I + \epsilon$) so that the threshold coefficient B_{ln^*} at $E = E_{n^*} (> E_I + \epsilon)$ is out of the flat top and exists on the upper cliff of the plateau. Thus, $|B_{ln^*}|$ takes an exponentially small value compared with those on the flat top of the plateau, and so does the tunneling amplitude caused by noninstanton tunneling. Therefore, the tunneling amplitude of the mutiphoton-assisted tunneling is determined by how steep the slope of the cliff is.

At a glance, the two interpretations of noninstanton tunneling, SUMGT and multiphoton-assisted tunneling, are quite different, but they predict essentially the same change of the tunneling amplitude as ω going to zero, i.e., the exponential decay. From the semiclassical viewpoint, the imaginary depths of SUMGT trajectories are inversely proportional to ω in the low-frequency range, and so do the imaginary parts of their classical actions. It induces the exponential decay of the tunneling amplitude in the limit $\omega \to 0$. On the other hand, the cliff of the plateau distribution of $|B_{ln}|$ becomes steeper exponentially in the limit $\omega \to 0$, and then the magnitude of the threshold coefficient $|B_{ln^*}|$ and the tunneling amplitude decay exponentially. Since the tunneling amplitude generated by instanton-type tunneling (barrier penetration) is almost constant independently of ω in the low-frequency range, then instanton-type tunneling overwhelms noninstanton tunneling below a threshold frequency at which the tunneling amplitude of noninstanton tunneling is equal to that of instanton-type tunneling, while noninstanton tunneling takes the maximum in the middle range above the threshold frequency.

In the low-frequency range, the localized tunneling spectrum generated by instanton-type tunneling satisfies the scaling law with respect to the width of the spectrum envelope, i.e., the width $\propto \hbar\omega$. In the case of the periodically perturbed rectangular barrier, the adiabatic approximation based on the unperturbed solution clarifies the following facts. The heights of the spectrum peaks $|T_n|$ at the same number n are independent of ω; $|T_0|$ is estimated as "the unperturbed

tunneling amplitude" $\times[1+O(\epsilon^2/\hbar^2)]$ and $|T_n|$ decays with $|n|$ as $|T_n/T_0| \propto 1/|n|!$. Then the width of the spectrum envelope changes proportionally to $\hbar\omega$, because the interval of the nearest peaks is $\hbar\omega$. This scaling law is necessary to preserve the transmissive probability in the limit $\omega \to 0$, otherwise the quantum probability diverges or decays unphysically. For the periodically perturbed Eckart barrier, the adiabatic approximation based on the instanton is available, and we get essentially the same result for instanton-type tunneling.

In the high-frequency range ($\omega > \omega_{cq}$), the tunneling phenomena are mainly ruled by the component of the fundamental energy level at $E = E_I$ caused by instanton-type tunneling and that of the first excited energy level at $E = E_I + \hbar\omega$ due to single-photon-assisted tunneling. The first excited level is larger in tunneling amplitude than the fundamental energy level when ω is just above ω_{cq}. However, the transition rates from the fundamental to excited energy levels decay monotonically with ω, while the tunneling amplitude of the fundamental converges on that of the unperturbed system in the limit $\omega \to \infty$. Therefore the total tunneling amplitude converges on that of the unperturbed system. The decay rate of the first excited energy level depends on the potential shape: the power law decay($\propto 1/\omega$) for the rectangular barrier, but the exponential decay for the rounded-off barrier.

As a consequence, we get the comprehensive scenario of tunneling phenomena observed for the periodically perturbed barriers in the whole range of the perturbation frequency from the semiclassical and quantum viewpoints. Application to two or more dimensional potential barriers and extension for the case that resonance tunneling occurs are problems for future research. For two or more dimensional potential barriers, many interesting approaches have been proposed providing successful results from rigorous and practical requirements, e.g., the reaction operator combined with visualization using the Weyl symbol [7], the semiclassical transition state theory [35,36] and the quantum instanton model [37]. It is an important problem to clarify the relation between our approach and those, especially for noninstanton tunneling in the semiclassical regime, i.e., SUMGT.

ACKNOWLEDGMENT

The present work is supported by Grant-in-Aid for Scientific Research (B) No. 24340094 from JSPA.

APPENDIX A: SOLUTION OF THE UNPERTURBED RECTANGULAR BARRIER

In this Appendix, we obtain the solution of the unperturbed rectangular barrier. The input, reflective and transmissive waves are, respectively, written as

$$\Psi_I = \mathrm{e}^{-\frac{i}{\hbar}E_I t}\mathrm{e}^{-\frac{i}{\hbar}P_I Q}, \tag{A1}$$

$$\Psi_R = R\mathrm{e}^{-\frac{i}{\hbar}E_I t}\mathrm{e}^{\frac{i}{\hbar}P_I Q}, \tag{A2}$$

$$\Psi_T = T\mathrm{e}^{-\frac{i}{\hbar}E_I t}\mathrm{e}^{-\frac{i}{\hbar}P_I Q}, \tag{A3}$$

where $P_I = \sqrt{2E_I}$. In the interaction region($b_w < Q < 0$), the left- and right-going waves are, respectively, given by

$$\Psi_l = B_l\mathrm{e}^{-\frac{i}{\hbar}E_I t}\mathrm{e}^{-\frac{i}{\hbar}P_b Q}, \tag{A4}$$

$$\Psi_r = B_r\mathrm{e}^{-\frac{i}{\hbar}E_I t}\mathrm{e}^{\frac{i}{\hbar}P_b Q}, \tag{A5}$$

where $P_b = \sqrt{2(E_I-1)}$ for $E_I > 1$ and $P_b = i\sqrt{2(1-E_I)}$ for $E_I < 1$.

Imposing continuity conditions on the wave at the boundaries, $Q = 0$ and $Q = b_w$, we obtain the coefficients, B_l, B_r, R, and T. The continuity at $Q = 0$ gives

$$1 + R = B_l + B_r \tag{A6}$$

and the continuous differentiability is written as

$$(-1+R)P_I = P_b(B_r - B_l). \tag{A7}$$

From the continuity at $Q = b_w = -|b_w|$, we get

$$T\mathrm{e}^{\frac{i}{\hbar}P_I|b_w|} = B_l\mathrm{e}^{\frac{i}{\hbar}P_b|b_w|} + B_r\mathrm{e}^{-\frac{i}{\hbar}P_b|b_w|} \tag{A8}$$

and from the continuous differentiability, we obtain

$$-P_I T\mathrm{e}^{\frac{i}{\hbar}P_I|b_w|} = -P_b B_l\mathrm{e}^{\frac{i}{\hbar}P_b|b_w|} + P_b B_r\mathrm{e}^{-\frac{i}{\hbar}P_b|b_w|}. \tag{A9}$$

Combining Eq. (A8) with Eq. (A9) gives

$$B_r = -\frac{P_I - P_b}{P_I + P_b}\mathrm{e}^{\frac{i}{\hbar}2P_b|b_w|}B_l. \tag{A10}$$

From Eqs. (A6) and (A7), we get

$$(P_I + P_b)B_l + (P_I - P_b)B_r = 2P_I. \tag{A11}$$

Substitution of Eq. (A10) into Eq. (A11) gives

$$B_l = \frac{2P_I}{(P_I + P_b) - \frac{(P_I-P_b)^2}{P_I+P_b}\mathrm{e}^{\frac{i}{\hbar}2P_b|b_w|}} \tag{A12}$$

and we get the reflective and transmissive coefficients from Eqs. (A6) and (A8). For the case that $E_I < 1$ and $\exp(-\frac{2}{\hbar}|P_b||b_w|) \ll 1$, Eqs. (A12) and (A8) are approximated as

$$B_l = \frac{2P_I}{(P_I + P_b) - \frac{(P_I-P_b)^2}{P_I+P_b}\mathrm{e}^{-\frac{2}{\hbar}|P_b||b_w|}} \sim \frac{2P_I}{P_I + P_b}, \tag{A13}$$

$$\begin{aligned} T &= \mathrm{e}^{-\frac{i}{\hbar}P_I|b_w|}\left(B_l\mathrm{e}^{-\frac{1}{\hbar}|P_b||b_w|} + B_r\mathrm{e}^{\frac{1}{\hbar}|P_b||b_w|}\right) \\ &\sim \mathrm{e}^{-\frac{i}{\hbar}P_I|b_w|}\mathrm{e}^{-\frac{1}{\hbar}|P_b||b_w|}\frac{4P_I P_b}{(P_I + P_b)^2}. \end{aligned} \tag{A14}$$

APPENDIX B: SOLUTION OF THE PERIODICALLY PERTURBED RECTANGULAR BARRIER IN THE HIGH-FREQUENCY RANGE

In the range $\omega > \omega_{cq}$, only the two components T_0 and T_1 are important to determine the tunneling amplitude. To estimate T_0 and T_1, we take into account only the terms of the

fundamental and first excited states in Eqs. (17) and (18):

$$i^0 J_0\left(\frac{\epsilon}{\hbar\omega}\right)[(P_{r0}+P_{b0})B_{l0}+(P_{r0}-P_{b0})B_{r0}]+iJ_1\left(\frac{\epsilon}{\hbar\omega}\right)[(P_{r0}+P_{b1})B_{l1}+(P_{r0}-P_{b1})B_{r1}]=2P_I, \tag{B1}$$

$$i^{-1} J_{-1}\left(\frac{\epsilon}{\hbar\omega}\right)[(P_{r1}+P_{b0})B_{l0}+(P_{r1}-P_{b0})B_{r0}]+i^0 J_0\left(\frac{\epsilon}{\hbar\omega}\right)[(P_{r1}+P_{b1})B_{l1}+(P_{r1}-P_{b1})B_{r1}]=0, \tag{B2}$$

and

$$\begin{aligned} &i^0 J_0\left(\frac{\epsilon}{\hbar\omega}\right)[(P_{t0}-P_{b0})e^{\frac{i}{\hbar}P_{b0}|b_w|}B_{l0}+(P_{t0}+P_{b0})e^{-\frac{i}{\hbar}P_{b0}|b_w|}B_{r0}] \\ &\quad +iJ_1\left(\frac{\epsilon}{\hbar\omega}\right)[(P_{t0}-P_{b1})e^{\frac{i}{\hbar}P_{b1}|b_w|}B_{l1}+(P_{t0}+P_{b1})e^{-\frac{i}{\hbar}P_{b1}|b_w|}B_{r1}]=0, \end{aligned} \tag{B3}$$

$$\begin{aligned} &i^{-1} J_{-1}\left(\frac{\epsilon}{\hbar\omega}\right)[(P_{t1}-P_{b0})e^{\frac{i}{\hbar}P_{b0}|b_w|}B_{l0}+(P_{t1}+P_{b0})e^{-\frac{i}{\hbar}P_{b0}|b_w|}B_{r0}] \\ &\quad +i^0 J_0\left(\frac{\epsilon}{\hbar\omega}\right)[(P_{t1}-P_{b1})e^{\frac{i}{\hbar}P_{b1}|b_w|}B_{l1}+(P_{t1}+P_{b1})e^{-\frac{i}{\hbar}P_{b1}|b_w|}B_{r1}]=0. \end{aligned} \tag{B4}$$

By using the approximations for $\frac{\epsilon}{\hbar\omega}\ll 1$, $J_0(\frac{\epsilon}{\hbar\omega})\sim 1$ and $J_{\pm1}(\frac{\epsilon}{\hbar\omega})\sim\pm\frac{\epsilon}{2\hbar\omega}$, B_{l0}, B_{r0}, B_{l1}, and B_{r1} are obtained as

$$B_{l0}\sim\frac{2P_I}{P_I+i|P_{b0}|}, \tag{B5}$$

$$\begin{aligned} B_{r0}\sim&-\frac{2P_I(P_I-i|P_{b0}|)}{(P_I+i|P_{b0}|)^2}e^{-\frac{2}{\hbar}|P_{b0}||b_w|}-\left(\frac{\epsilon}{2\hbar\omega}\right)^2 e^{-\frac{1}{\hbar}|P_{b0}||b_w|}e^{\frac{i}{\hbar}P_{b1}|b_w|}2P_I \\ &\times\frac{(P_{t1}-i|P_{b0}|)[(P_I-i|P_{b0}|)(P_I-P_{b1})-(P_I-P_{b1})(P_{t1}+P_{b1})]}{(P_I+i|P_{b0}|)^2\left[(P_{t1}+P_{b1})^2-(P_{t1}-P_{b1})^2e^{\frac{i}{\hbar}2P_{b1}|b_w|}\right]}, \end{aligned} \tag{B6}$$

$$B_{l1}\sim-i\left(\frac{\epsilon}{2\hbar\omega}\right)\frac{2P_I(P_{t1}+i|P_{b0}|)(P_{t1}+P_{b1})}{(P_I+i|P_{b0}|)\left[(P_{t1}+P_{b1})^2-(P_{t1}-P_{b1})^2e^{\frac{i}{\hbar}2P_{b1}|b_w|}\right]}, \tag{B7}$$

$$B_{r1}\sim i\left(\frac{\epsilon}{2\hbar\omega}\right)e^{\frac{i}{\hbar}2P_{b1}|b_w|}\frac{2P_I(P_{t1}+i|P_{b0}|)(P_{t1}-P_{b1})}{(P_I+i|P_{b0}|)\left[(P_{t1}+P_{b1})^2-(P_{t1}-P_{b1})^2e^{\frac{i}{\hbar}2P_{b1}|b_w|}\right]}. \tag{B8}$$

Then T_0 and T_1 are given by

$$\begin{aligned} T_0&\sim e^{-\frac{i}{\hbar}P_I|b_w|}\left[e^{-\frac{1}{\hbar}|P_{b0}||b_w|}B_{l0}+e^{\frac{1}{\hbar}|P_{b0}||b_w|}B_{r0}+i\frac{\epsilon}{2\hbar\omega}\left(e^{\frac{i}{\hbar}P_{b1}|b_w|}B_{l1}+e^{-\frac{i}{\hbar}P_{b1}|b_w|}B_{r1}\right)\right] \\ &\sim e^{-\frac{i}{\hbar}P_I|b_w|}\left(e^{-\frac{1}{\hbar}|P_{b0}||b_w|}\frac{4iP_I|P_{b0}|}{(P_I+i|P_{b0}|)^2}-\left(\frac{\epsilon}{2\hbar\omega}\right)^2 e^{\frac{i}{\hbar}P_{b1}|b_w|}2P_I\right. \\ &\quad\times\left\{\frac{(P_{t1}-i|P_{b0}|)[(P_I-i|P_{b0}|)(P_I-P_{b1})-(P_I-P_{b1})(P_{t1}+P_{b1})]}{(P_I+i|P_{b0}|)^2[(P_{t1}+P_{b1})^2-(P_{t1}-P_{b1})^2e^{\frac{i}{\hbar}2P_{b1}|b_w|}]}\right. \\ &\quad\left.\left.-\frac{2(P_{t1}+i|P_{b0}|)P_{b1}}{(P_I+i|P_{b0}|)[(P_{t1}+P_{b1})^2-(P_{t1}-P_{b1})^2e^{\frac{i}{\hbar}2P_{b1}|b_w|}]}\right\}\right) \\ &\sim e^{-\frac{i}{\hbar}P_I|b_w|}\left[e^{-\frac{1}{\hbar}|P_{b0}||b_w|}\frac{4iP_I|P_{b0}|}{(P_I+i|P_{b0}|)^2}+\left(\frac{\epsilon}{2\hbar\omega}\right)^2 e^{\frac{i}{\hbar}P_{b1}|b_w|}2P_I f(E_I)\right] \end{aligned} \tag{B9}$$

and

$$\begin{aligned} T_1&\sim e^{-\frac{i}{\hbar}P_{t1}|b_w|}\left[i\frac{\epsilon}{2\hbar\omega}\left(e^{-\frac{1}{\hbar}|P_{b0}||b_w|}B_{l0}+e^{\frac{1}{\hbar}|P_{b0}||b_w|}B_{r0}\right)+e^{\frac{i}{\hbar}P_{b1}|b_w|}B_{l1}+e^{-\frac{i}{\hbar}P_{b1}|b_w|}B_{r1}\right] \\ &\sim -ie^{-\frac{i}{\hbar}(P_{t1}-P_{b1})|b_w|}\frac{2\epsilon}{\hbar\omega}P_IP_{b1}\frac{P_{t1}+i|P_{b0}|}{(P_I+i|P_{b0}|)[(P_{t1}+P_{b1})^2-(P_{t1}-P_{b1})^2e^{\frac{i}{\hbar}2P_{b1}|b_w|}]} \\ &\sim -ie^{-\frac{i}{\hbar}(P_{t1}-P_{b1})|b_w|}\frac{2\epsilon}{\hbar\omega}P_IP_{b1}g(E_I)\sim O\left(\frac{\epsilon}{\hbar\omega}\right), \end{aligned} \tag{B10}$$

where $f(E_I)=\tilde{f}(P_I(E_I),P_{b0}(E_I),P_{b1}(E_I),P_{t1}(E_I))$ and $g(E_I)=\tilde{g}(P_I(E_I),P_{b0}(E_I),P_{b1}(E_I),P_{t1}(E_I))$ are functions of $O(1)$.

[1] S. Tomsovic, editor, *Tunneling in Complex Systems* (World Scientific, Singapore 1998).

[2] J. Ankerhold, *Quantum Tunneling in Complex Systems: The Semiclassical Approach* (Springer-Verlag, Berlin, Heidelberg, 2007).

[3] S. Keshavamurthy, Int. Rev. Phys. Chem. **26**, 521 (2007).

[4] S. Keshavamurthy and P. Schlagheck, editors, *Dynamical Tunneling: Theory and Experiment* (CRC Press, Boca Raton, FL, 2011).

[5] O. Bohigas, S. Tomsovic, and D. Ullmo, Phys. Rev. Lett. **65**, 5 (1990); Phys. Rep. **223**, 45 (1993).

[6] S. C. Creagh and N. D. Whelan, Phys. Rev. Lett. **84**, 4084 (2000).

[7] S. C. Creagh, Nonlinearity **17**, 1261 (2004); **18**, 2089 (2005); C. S. Drew, S. C. Creagh, and R. H. Tew, Phys. Rev. A **72**, 062501 (2005).

[8] W. K. Hensinger *et al.*, Nature (London) **412**, 52 (2001); D. A. Steck, W. H. Oskay, and M. G. Raizen, Science **293**, 274 (2001); C. Dembowski, H.-D. Gräf, A. Heine, R. Hofferbert, H. Rehfeld, and A. Richter, Phys. Rev. Lett. **84**, 867 (2000).

[9] O. Brodier, P. Schlagheck, and D. Ullmo, Phys. Rev. Lett. **87**, 064101 (2001); Ann. Phys. (NY) **300**, 88 (2002); C. Eltschka and P. Schlagheck, Phys. Rev. Lett. **94**, 014101 (2005).

[10] A. Bäcker, R. Ketzmerick, S. Löck, and L. Schilling Phys. Rev. Lett. **100**, 104101 (2008); A. Bäcker, R. Ketzmerick, S. Löck, M. Robnik, G. Vidmar, R. Höhmann, U. Kuhl, and H.-J. Stöckmann, *ibid.* **100**, 174103 (2008); A. Bäcker, R. Ketzmerick, S. Löck, J. Wiersig, and M. Hentschel, Phys. Rev. A **79**, 063804 (2009); S. Löck, A. Bäcker, R. Ketzmerick, and P. Schlagheck, Rhys. Rev. Lett. **104**, 114101 (2010).

[11] A. Shudo and K. S. Ikeda, Phys. Rev. Lett. **74**, 682 (1995); Physica D **115**, 234 (1998); T. Onishi, A. Shudo, K. S. Ikeda, and K. Takahashi, Phys. Rev. E **64**, 025201(R) (2001); **68**, 056211 (2003).

[12] A. Shudo, Y. Ishii, and K. S. Ikeda, J. Phys. A **35**, L225 (2002); Europhys. Lett. **81**, 50003 (2008); J. Phys. A **42**, 265101 (2009); **42**, 265102 (2009).

[13] K. Takahashi, A. Yoshimoto, and K. S. Ikeda, Phys. Lett. A **297**, 370 (2002); K. Takahashi and K. S. Ikeda, J. Phys. A **36**, 7953 (2003).

[14] K. Takahashi and K. S. Ikeda, Europhys. Lett. **71**, 193 (2005); **75**, 355 (2006) (erratum).

[15] K. Takahashi and K. S. Ikeda, J. Phys. A. **41**, 095101 (2008).

[16] K. Takahashi and K. S. Ikeda, Phys. Rev. A **79**, 052114 (2009).

[17] K. Takahashi and K. S. Ikeda, J. Phys. A **43**, 192001 (2010).

[18] K. Takahashi and K. S. Ikeda, Phys. Rev. Lett. **97**, 240403 (2006); **107**, 219903(E) (2011).

[19] K. Takahashi and K. S. Ikeda, Phys. Rev. E **84**, 026203 (2011).

[20] L. S. Schulman, *Techinques and Applications of Path Integration* (John Wiley, New York, 1981).

[21] F. Bezrukov and D. Levkov, J. Exper. Theor. Phys. **98**, 820 (2004); D. G. Levkov, A. G. Panin, and S. M. Sibiryakov, Phys. Rev. Lett. **99**, 170407 (2007); Phys. Rev. E **76**, 046209 (2007); J. Phys. A **42**, 205102 (2009).

[22] J. Y. Ge and J. Z. H. Zhang, J. Chem. Phys. **105**, 8628 (1996).

[23] M. Büttiker and R. Landauer, Phys. Rev. Lett. **49**, 1739 (1982); Phys. Scr. **32**, 429 (1985).

[24] W. J. Li and L. E. Reichl, Phys. Rev. B **60**, 15732 (1999).

[25] A. Pimpale, S. Holloway, and R. J. Smith, J. Phys. A **24**, 3533 (1991).

[26] M. J. Hagmann, J. Appl. Phys. **78**, 25 (1995).

[27] M. Garttner, F. Lenz, C. Petri, F. K. Diakonos, and P. Schmelcher, Phys. Rev. E **81**, 051136 (2010).

[28] K. Takahashi and K. S. Ikeda, J. Chem. Phys. **106**, 4463 (1997).

[29] W. H. Miller, J. Chem. Phys **53**, 1949 (1970); Adv. Chem. Phys. **25**, 69 (1974).

[30] K. Takahashi, "Semiclassical Analysis of Multidimentional Barrier Tunneling," section 5 of Ref. [4].

[31] M. Abramowitz and I. A. Stegun, *Handbook of Mathematical Functions* (Dover Publications, New York, 1965).

[32] K. Takahashi and K. S. Ikeda, Ann. Phys. (NY) **283**, 94 (2000).

[33] V. K. Melnikov, Trans. Moscow Math. Soc. **12**, 1 (1963).

[34] S. Wiggins, *Introduction to Applied Nonlinear Dynamical Systems and Chaos* (Springer-Verlag, New York, 1990).

[35] W. H. Miller, and R. Hernandez, N. C. Handy, D. Jayatilaka, and A. Willetts, Chem. Phys. Lett. **172**, 62 (1990).

[36] T. L. Nguyen, J. F. Stanton, and J. R. Barker, J. Phys. Chem. A **115**, 5118 (2011); J. R. Barker, T. L. Nguyen, and J. F. Stanton, *ibid.* **116**, 6408 (2012); T. L. Nguyen, B. C. Xue, R. E. Weston, Jr., J. R. Barker, and J. F. Stanton, J. Phys. Chem. Lett. **3**, 1549 (2012).

[37] W. H. Miller, Y. Zhao, M. Ceotto, and S. Yang, J. Chem. Phys. **119**, 1329 (2005).